

Role of chain stiffness on the conformation of single polyelectrolytes in salt solutions

Yu-Fu Wei and Pai-Yi Hsiao*

*Department of Engineering and System Science,
National Tsing Hua University, Hsinchu, Taiwan 300, R.O.C.*

(Dated: February 8, 2022)

Abstract

Conformation of single polyelectrolytes in tetravalent salt solutions is investigated under the framework of a coarse-grained model, using Langevin dynamics simulations. The chain size, studied by the radius of gyration, shows three different variational behaviors with salt concentration, depending on the chain stiffness. According to the size variations, polyelectrolytes of fixed chain length are classified into three categories: (1) flexible chain, for which the variation shows a curve similar to a tilted letter L; (2) semiflexible chain, whose curve looks resemble of the letter U; (3) rigid chain, for which the curve is a straight line. The worm-like chain model with persistence length predicted by the Odijk-Skolnick-Fixman theory is found to be able to qualitatively describe the end-to-end distance at low salt concentration, not only for semiflexible and rigid chains but also for flexible chain. In a low-salt region, a flexible polyelectrolyte extends more significantly than a semiflexible chain, in reference of the size of their uncharged counterparts, and in a high-salt region, regardless of chain stiffness, a chain attains a dimension comparable to that of its neutral polymer. The chain stiffness influences both the local and the global chain structures. A flexible chain exhibits a zigzagged local structure in the presence of salt ions and the condensed structure is a disordered, random globule. A semiflexible chain is locally smooth, and the condensed structure is orderly packed, taking a form such as hairpin or toroid. Moreover, the chain stiffness can also affect the nature of the coil-globule transition. The transition is occurred in a discrete manner for semiflexible chain, whereas in a continuous way for flexible chain. This discrete feature is happened not only at low salt concentration when a semiflexible chain is collapsed, but also at high salt concentration when the collapsed chain is reexpanded. At the end, the effects of chain stiffness and salt concentration on the conformation of single polyelectrolytes are summarized in a schematic state diagram.

PACS numbers:

*Corresponding author. E-mail: pyhsiao@ess.nthu.edu.tw

I. INTRODUCTION

There is a resurgent interest in studying the properties of polyelectrolytes in multivalent salt solutions because such system reveals many fascinating phenomena. One vital example is the DNA condensation, in which DNA, a negatively-charged polyelectrolyte, undergoes a dramatic condensation from an extended structure to a compact, highly-ordered structure while multivalent salt is added to the solution [1, 2, 3, 4]. The condensation induced by multivalent salt is not a privilege reserved only for DNA but a common feature of polyelectrolytes [5, 6, 7]. Usually trivalent salts or charged molecules of higher valence are demanded to induce the condensation [3, 8]. Experiments have shown that the morphology of the condensate depends strongly on the chain bending rigidity which balances the attractive collapsing force at a solvent quality. Flexible polymers generally collapse to disordered globules, and stiff ones collapse to ordered structures such as toroid or folded chain [2, 7, 9]. The influence of chain stiffness on chain morphology has been investigated by simulations, including the condensation of polyelectrolyte induced by multivalent salt [10] or by increasing Coulomb strength parameter [11] and the collapse of neutral polymer driven by temperature decrease [12, 13]. The results confirmed that chain rigidity plays a decisive role in determination of the condensed structure.

A phenomenon which is less well-known appears when an excess of multivalent salt is presented in the solution: The salt-induced condensation redissolves into the solution and the system returns to a homogeneous phase [5, 6, 14]. This phenomenon is called “reentrant condensation” [15] and has been discovered since seventy-five years ago in the study of the coacervation of colloids by oppositely charged ions [16]. It occurs for flexible chains, for example, polystyrene sulphonate [5], and also for stiff chains, for example, DNA [6]. The persistence length in the latter example is two order of magnitude larger than in the previous. As the condensation takes place, the bare chain charge is almost neutralized by the condensed counterions dissociated from the multivalent salt [17, 18]. These counterions not only screens out the long-range Coulomb repulsion but also creates a short-range attraction due to correlated fluctuation, resulting in the condensation [19, 20]. On the other hand, for the redissolution of polyelectrolytes at high salt concentration, no comprehensive explanation is well established. Recently, two theories were proposed to explain the phenomenon but verification is still ongoing. The first theory suggested that the redissolution is a consequence

of charge inversion occurring when polyelectrolyte binds so many counterions that its net charge alters sign [15, 21], whereas the second one argued that it has an origin of the screening of the short-range attraction [22, 23]. The second theory, furthermore, predicted that Bjerrum association plays an important role on the organization of polyelectrolyte-ion complexes [24], and therefore, charge reversal is not always happened.

The folding transition of a polymer between an elongated state and a compact state is called “coil-globule transition” [25]. Theorists predicted that for semiflexible chains, such transition is first order, using mean-field theory [25, 26, 27]. The prediction has been confirmed experimentally [28, 29]. Despite continuous for the whole ensemble, the coil-globule transition is discrete at the level of single chain for polymers with sufficient stiffness [29]. In this case, the transition is similar to the disordered-ordered transition between a gas-like and a crystal-like state. On the other hand, for single polymers with small stiffness, the transition is continuous, resembling to the disordered-disordered transition between a gas-like and a liquid-like state. This topic has been recently studied in simulations [10, 11, 12, 13]. The results showed that the discrete transition can be induced by adding condensing agent [10] or by decreasing temperature [12, 13], while chains are stiff. However, the discussions were mainly focused on the chain condensation occurring in low temperature region or in low salt regime. Since an excess of multivalent salt can lead condensed chains reentering into the solution, it becomes very relevant to know whether the reentering transition behaves in a discrete manner or not. To our knowledge, there is no simulation nor experiment, hitherto, discussing the conformational transition on the chain reentrance occurring at high salt concentrations. To get insight of it, we investigate in this paper the behavior of single polyelectrolytes with addition of multivalent salt by means of computer simulation. The salt covers a broad range of concentration so that single chains show, in turn, the condensation and the reentrance transitions in a microscopic way. Our study, therefore, offers a good opportunity to investigate thoroughly the coil-globule transition happened at low and at high salt concentrations.

There have been many simulations devoting to the study of the behavior of polyelectrolytes in salt-free solutions [11, 30, 31, 32, 33, 34, 35, 36, 37, 38, 39, 40]. Only recently, the study with addition of salt becomes numerically feasible because of the progress of computing power. However, the salt valence studied in the literatures was usually monovalent or divalent [41, 42, 43, 44]. For the study with high salt valence, the focus was mainly on the

condensation of polyelectrolyte and the salt concentration was not high enough to investigate the chain reentrance into a solution [10, 45, 46, 47]. One indirect way to discuss DNA condensation and redissolution is to measure the effective interaction between two immobile rigid polyelectrolytes in the environment of multivalent salt [39, 48]. Recently, progress has been made in a series of study [49, 50, 51]: By carefully choosing the simulation parameters, we were able to investigate salt-induced condensation and redissolution thoroughly in a direct way. We found that the dimension of flexible polyelectrolytes undergoes subsequently two continuous transitions upon addition of multivalent salt, the collapsing transition and the swelling transition, which are respectively the microscopic representation of the condensation and the redissolution of polyelectrolyte. We demonstrated that the excluded volume of ion plays an imperative role on the chain properties and should be inevitably incorporated in a theoretical analysis [49, 50]. The study of the potential of mean force showed that like-charge attraction between chains happens only when salt concentration is intermediate around *the equivalence point* (see Sec. III A for definition) and the size ratio of ion to monomer lies within a window around unity [50]. Moreover, it was shown that only salt valence greater than two can induce apparently the two structural transitions [51], which is consistent with experimental observations [1, 6, 17, 52]. Nonetheless, the effect of chain stiffness was not discussed in these studies. Since semiflexible polyelectrolytes exhibit several intriguing phenomena, not being seen in flexible polymers, we focus in this work how chain stiffness influences chain morphology.

Toroid structure is presumed to be the ground state of a compacted DNA [3, 53]. However, folded-rod structure and a number of other morphology, such as racquet, are also often observed in experiments [54, 55, 56]. The long lifetime of some of these structures indicates that DNA has complicated energy landscape. Numerical studies showed that the energy levels of toroid and rodlike structure are comparable [12, 35]. These two structures are surrounded by many metastable states and hindered by high energy barriers. Debate continues until now in deciding which structure is the real ground state of a condensed DNA and under what condition it applies. One of the important factors which affects the chain morphology is the chain length. It was observed that longer chains display higher appearance percentage for toroids than for rods [2, 57, 58]. Also, the degree of ion condensation on a chain was found to increase with chain length [59, 60]. Recently, chain length effect on the state diagram of a single chain has been discussed [61]. Limited to today's computational power,

time period able to be studied by molecular simulations is very short. It is, thus, difficult to investigate properly the evolution of chain morphology, because of the long lifetime of some of the chain structures. Therefore, many authors found that the formation of a toroidal or a rod-like structure pertains to the initial chain configuration used in simulations [11, 12, 35]. In this article, we study the morphology of a single polyelectrolyte with fixed chain length. For the chain stiffness in which the morphological evolution is slow, several simulations are performed, starting with different initial configurations, to make sampling more complete. By this way, we calculate static properties. The rest of the article is organized as follows. The simulation model and the method used in this study are described in Sec. II. The results and discussions are given in Sec. III. The topics include the radius of gyration (Sec. III A), the degree of chain swelling (Sec. III B), the end-to-end distance (Sec. III C), the probability density distribution (Sec. III E), and the dynamics of chain conformation (Sec. III F). Simulation snapshots are presented in Sec. III D. We summarize the conformation of a single polyelectrolyte in a state diagram in Sec. III G and give our conclusions in Sec. IV.

II. MODEL AND SIMULATION METHOD

Our system consists of a single polyelectrolyte modeled by a negatively charged bead-spring chain and spherical counterions dissociated from the chain. There are 48 beads (monomers) on the chain. Each of the beads carries a $-e$ charge and each of the counterions carries a $+e$ charge. Tetravalent salt is added into the system. It is dissociated into tetravalent cations (counterions) and monovalent anions (coions), modeled by charged spheres. Solvent molecules are not incorporated explicitly in the simulations. We suppose them forming a medium of constant dielectric constant ϵ_r . The collision between particles and solvent molecules is considered, and the effect is described by Langevin equation. The system is placed in a cubic box and periodic boundary condition is applied.

Four types of interaction are involved in the simulations. The first one is the excluded-volume interaction, which is applied for all the particles, including monomers, counterions and coions. It is modeled by a purely repulsive Lennard-Jones (LJ) potential

$$U_{ex}(r) = \begin{cases} 4\varepsilon_{LJ} [(\sigma/r)^{12} - (\sigma/r)^6] + \varepsilon_{LJ} & \text{for } r \leq 2^{1/6}\sigma \\ 0 & \text{for } r > 2^{1/6}\sigma \end{cases} \quad (1)$$

where ε_{LJ} is the interaction strength and σ is the diameter of a particle. The second

interaction is the Coulomb interaction $U_{coul}(r) = Z_i Z_j e^2 / (4\pi\epsilon_0\epsilon_r r)$ where Z_i and Z_j are respectively the valences of particle i and j , ϵ_0 is the permittivity in vacuum, ϵ_r is the dielectric constant of the medium. It can be re-expressed as

$$U_{coul}(r) = \frac{Z_i Z_j \lambda_B k_B T}{r} \quad (2)$$

where k_B is the Boltzmann constant, T is the temperature, and $\lambda_B = e^2 / (4\pi\epsilon_0\epsilon_r k_B T)$ is the Bjerrum length, which denotes the distance between two unit charges at which the Coulomb energy is equal to the thermal energy $k_B T$. The third interaction is the bond connectivity interaction. Two adjacent monomers are connected by a *spring*, modeled by a finitely extensible nonlinear elastic potential

$$U_{bond}(b) = -\frac{1}{2} k_b b_{max}^2 \ln \left(1 - \frac{b^2}{b_{max}^2} \right) \quad (3)$$

where b is the length of a bond, b_{max} is the maximum bond extention, and k_b is the spring constant. The forth interaction is a harmonic angle potential, which gives chain stiffness,

$$U_{angle}(\theta) = k_a (\theta - \theta_0)^2 \quad (4)$$

where θ is the angle between two consecutive bonds, θ_0 is the equilibrium angle, and k_a is the force constant.

We perform Langevin dynamics simulations in this study. The equation of motion of a particle i is described by the stochastic differential equation

$$m_i \ddot{\vec{r}}_i = -\frac{\partial U}{\partial \vec{r}_i} - m_i \gamma_i \dot{\vec{r}}_i + \vec{\eta}_i(t) \quad (5)$$

where m_i is the mass of particle i , $m_i \gamma_i$ denotes the friction coefficient and $\vec{\eta}_i$ is a random force modeling the collisions by solvent molecules. $\vec{\eta}_i(t)$ has zero mean over time and satisfies the fluctuation-dissipation theorem:

$$\langle \vec{\eta}_i(t) \cdot \vec{\eta}_j(t') \rangle = 6k_B T m_i \gamma_i \delta_{ij} \delta(t - t') \quad (6)$$

where δ_{ij} and $\delta(t - t')$ are the Kronecker delta and the Dirac delta function, respectively. An advantage of using Langevin dynamics is that the temperature control is naturally incorporated.

In this work, we assume that all the particles have identical mass m , diameter σ , and LJ interaction strength ε_{LJ} . We set $\lambda_B = 3\sigma$ and control temperature at $k_B T = 1.2\varepsilon_{LJ}$.

Coulomb interaction is computed using the technique of Ewald sum. k_b is chosen to be $5.8333k_BT/\sigma^2$ and b_{max} to be 2σ . Under this setup, the average bond length is 1.1σ [31, 49]. We study the effect of chain stiffness by altering the spring constant k_a from 0 to $100k_BT/rad^2$. The equilibrium angle θ_0 is set to be π . The size of the simulation box is 53.133σ and the concentration of tetravalent salt ranges from 0.0 to $0.01024\sigma^{-3}$. All the particles are subjected to a friction force proportional to the particle velocity. We set the damping constant γ to $15.0\tau^{-1}$ to mimic roughly an aqueous environment where $\tau = \sigma\sqrt{m/(k_BT)}$ is the time unit. Simulation time step δt is chosen equal to 0.005τ . The initial chain configuration begins with an extended structure. An equilibrium phase takes 3×10^6 to 5×10^7 time steps and a production run 10^7 to 3×10^8 time steps, depending on chain stiffness and salt concentration. We found that in the region of intermediate salt concentration, the transition between different chain structures is slow. In order to sample more completely different structures, five to ten independent runs are performed starting with different initial configurations. The simulations were run using LAMMPS package [76]. For the case of the highest salt concentration, the system contains 7776 charged particles.

III. RESULTS AND DISCUSSIONS

A. Radius of gyration

The size of a polyelectrolyte can be characterized by the radius of gyration, R_g . It is calculated by taking the square root of the formula,

$$R_g^2 = \frac{1}{N} \sum_{i=1}^N (\vec{r}_i - \vec{r}_{cm})^2 \quad (7)$$

where N is the number of monomers on the chain, \vec{r}_i is the position vector of monomer i , and \vec{r}_{cm} is the center of mass of the chain. We studied the effects of salt concentration and chain stiffness on the root-mean-square radius of gyration, $\langle R_g^2 \rangle^{1/2}$. The results are shown in Fig.1.

We observed that the variation of $\langle R_g^2 \rangle^{1/2}$ behaves in three distinct manners. The first behavior applies to the chain with small k_a , such as $k_a = 0.0k_BT/rad^2$. $\langle R_g^2 \rangle^{1/2}$ firstly decreases with increasing C_s , the concentration of the tetravalent salt, until the total charge of the tetravalent cations is equal to the negative charge carried on the chain backbone. We

call this particular salt concentration *the equivalence point*. In this work, the equivalence point occurs at $C_s = C_s^* \equiv 8 \times 10^{-5} \sigma^{-3}$ because the monomer concentration is fixed at $C_m = 3.2 \times 10^{-4} \sigma^{-3}$. $\langle R_g^2 \rangle^{1/2}$ then increases slowly while C_s surpasses the equivalence point. Therefore, the chain undergoes two structural transitions upon addition of tetravalent salt: a shrinking transition and a followed swelling transition. The increasing rate of $\langle R_g^2 \rangle^{1/2}$ in the chain swelling region is apparently lower than the decreasing rate in the chain shrinking region. As a result, the curve of $\langle R_g^2 \rangle^{1/2}$ looks similar to a tilted ‘L’ in the semilog plot. Notice that at high salt concentration, the chain is not swollen back to its original size in the absence of salt. These phenomena have been recently studied in detail by molecular dynamics simulations [49, 50].

The second behavior applies to the chain with intermediate k_a , for instance, $k_a = 8.0 k_B T / rad^2$. At the beginning of addition of salt, the chain size decreases gently. The gentle decrease turns to become a sharp decrease once C_s is increased beyond some critical value C_c , and quickly, $\langle R_g^2 \rangle^{1/2}$ reaches a small constant value. If C_s is further increased over a second critical value C_d , an abrupt increase in $\langle R_g^2 \rangle^{1/2}$ takes place. The equivalence point C_s^* is situated in the region between C_c and C_d . In the high-salt region $C_s > C_d$, the chain reattains roughly its original size before the condensation occurred. These two sudden changes suggest that the chain morphology is altered, from an extended structure to a condensed structure, and vice versa, in a discontinuous way. The chain possibly commits a first-order conformational transition [12, 29]. In the semilog plot, the shape of the $\langle R_g^2 \rangle^{1/2}$ curve looks like the capital letter ‘U’. A relevant phenomenon has been observed in the experiments of DNA precipitation by polyamines where DNA percentage presented in the supernatant shows a similar U-shaped variation as a function of spermidine concentration [6, 62]. Suppose that the occurrence of the chain precipitation is directly related to the chain size in the solution. This variation will then reflect how the dimension of a semiflexible DNA varies with salt concentration. Our results are in agreement with the experimental observation.

The third behavior is observed for the chain with large k_a , for example, $k_a = 100 k_B T / rad^2$. The influence of the adding salts upon the chain size is not significant. $\langle R_g^2 \rangle^{1/2}$ stays essentially at a constant value, and in the figure, the curve is roughly a straight line.

Based upon the variation of chain size against C_s , a polyelectrolyte of fixed chain length can be classified into three categories according to the chain stiffness:

- (1) *flexible chain*, characterized by a tilted-L-shaped $\langle R_g^2 \rangle^{1/2}$ curve;
- (2) *semiflexible chain*, characterized by a U-shaped $\langle R_g^2 \rangle^{1/2}$ curve;
- (3) *rigid chain*, characterized by an almost straight $\langle R_g^2 \rangle^{1/2}$ curve.

One way to justify if a chain belongs to the category *rigid chain* or not is to compare the bare persistence length with the chain length. If the bare persistence length is larger than the chain length, the chain is considered to be *rigid*. In our study, the bare persistence length $\ell_{p,0}$ is related to the force constant k_a of the harmonic angle potential by $\ell_{p,0} = 2k_a \langle b \rangle / (k_B T)$ where $\langle b \rangle$ is the average bond length. Therefore, $\ell_{p,0}$ becomes larger than the chain length while $k_a > 24k_B T / \text{rad}^2$. This simple criterion works reasonably well because the chain shows a rigid rod structure at all C_s for $k_a = 30k_B T / \text{rad}^2$ and $100k_B T / \text{rad}^2$ but not for the cases with smaller k_a , as having been shown in Fig.1.

In the simulations, we observed that, no matter how stiff the chain is, the polyelectrolyte is in its most stretched state while no salt is added into the solution. We found that at a given salt concentration, a stiffer chain displays a larger $\langle R_g^2 \rangle^{1/2}$, and hence, occupies a larger space. The results obtained here also demonstrate that the chain stiffness plays an imperative role in the determination of the type of the coil-globule transition to be continuous or discrete, both in the condensation and in the reexpansion of a polyelectrolyte.

B. Degree of swelling

In order to understand the degree of swelling of a polyelectrolyte in salt solutions, we calculate the size of the uncharged counterpart of the polyelectrolyte in a salt-free solution and use it as the reference of comparison. The root-mean-square radius of gyration of the uncharged chain, $\langle R_{g,n}^2 \rangle^{1/2}$, is equal to 5.1(1), 12.1(2), and 14.97(6) for the cases $k_a = 0.0$, 8.0 and $100.0k_B T / \text{rad}^2$, respectively. We define the degree of chain swelling by $\alpha = (\langle R_g^2 \rangle^{1/2} / \langle R_{g,n}^2 \rangle^{1/2}) - 1$ and present the results in Fig. 2.

We observed that in the low-salt region, α is positive. It means that the charged chain occupies a larger space than the uncharged chain, apparently resulting from the electrostatic repulsion between monomers on the chain. The value of α for the flexible chain ($k_a = 0.0k_B T / \text{rad}^2$) is much larger than the ones for the semiflexible chain ($k_a = 8.0k_B T / \text{rad}^2$) and for the rigid chain ($k_a = 100.0k_B T / \text{rad}^2$). Therefore, the major contribution to the

dimension of a semiflexible or a rigid polyelectrolyte comes from the intrinsic chain stiffness, whereas the size of a flexible chain is mainly determined by the Coulomb repulsion on the chain backbone. In the mid-salt region around the equivalence point, the degree of swelling is negative for the flexible chain and for the semiflexible chain. The chains are, hence, in collapsed states. In this region, electrostatics dominates the chain stiffness. The maximum shrinkage, in reference of the size of the neutral chain, can be as large as 50%. For the rigid chain, the collapsing transition does not happen, and thus, α is close to zero. In the high-salt region, we saw that the value of α approaches to zero for the semiflexible chain. The polyelectrolyte hence occupies a space volume similar to its uncharged counterpart. For the flexible chain, α is increased with C_s but still takes a finite negative value. In our previous study [50], flexible polyelectrolytes in the region of much higher salt concentration have been investigated, and the results showed that the chain attains a size similar to the neutral polymers. Therefore, α is expected to tend toward zero if C_s was increased to a much higher value in the current study.

In Fig. 3, we present the variation of α as a function of k_a at different C_s . At small C_s , α is positive and monotonically decreases to zero with increasing k_a . Opposite trend of behavior is observed at large C_s , for instance, $C_s = 0.01024\sigma^{-3}$, where α is negative and monotonically increases to zero. In the mid-salt region, α displays a V-shaped curve and the maximum shrinkage is happened around $k_a = 5k_BT/rad^2$. Thus, by tuning k_a and varying C_s , one is able to control the degree of chain swelling to design desired functions in real applications.

The results obtained here tell us that in a salt-free solution, the larger the value of k_a , the less significant the size difference between a charged chain and its uncharged counterpart will be. Since at large C_s a chain occupies a space similar to the one of a neutral polymer, a semiflexible chain will regain roughly its original size at zero C_s by addition of many salts into the solution, but a flexible chain will not regain it.

C. End-to-end distance

Conventionally, the end-to-end distance R_e is used to characterize the size of a polymer. In Fig. 4 we present how the root-mean-square end-to-end distance, $\langle R_e^2 \rangle^{1/2} = \langle (\vec{r}_N - \vec{r}_1)^2 \rangle^{1/2}$, varies with salt concentration for different chain stiffness, where \vec{r}_1 and \vec{r}_N are the position

vectors of the two ends of a chain. The behavior of R_e resembles the behavior of R_g : a flexible chain displays a tilted L-shaped R_e curve, a semiflexible one displays a U-shaped R_e curve, and a rigid one displays a straight R_e curve. Nonetheless, the value of R_e does not precisely reflect the *real* size of a chain. For example, R_e for a semiflexible chain becomes smaller than that for a flexible chain in the mid-salt region, although a semiflexible chain has a larger size (cf. Fig. 1). This inconsistency results from the formation of ordered structures which gives a small R_e , such as hairpin or ring-like structure. Therefore, the quantity R_e is not always suitable to characterize the dimension of a chain in a salt solution, particularly when the chain stiffness is intermediate.

The mean-square end-to-end distance of a chain has been derived theoretically under the framework of the worm-like chain (WLC) model and reads as

$$\langle R_e^2 \rangle = 2\ell_p L - 2\ell_p^2 (1 - \exp(-L/\ell_p)) \quad (8)$$

where L is the contour length and ℓ_p is the persistence length [63]. For a polyelectrolyte chain, ℓ_p is the sum of two contributions: the first one is the bare persistence length $\ell_{p,0}$, coming from the intrinsic chain stiffness, and the second one is the electrostatic persistence length ℓ_e , due from the electrostatic interaction. Odijk [64] and, independently, Skolnick and Fixman [65] (OSF) have deduced a formula for the electrostatic persistence length in the limit of stiff chain and low ionic strength. This formula reads as

$$\ell_e^{OSF} = \frac{\xi^2}{4\kappa^2\lambda_B} \quad (9)$$

where ξ is the Manning parameter, defined as the ratio of λ_B over the effective charge distance on the chain, and κ is the inverse Debye length. In order to make a comparison of the simulation results with the theory, we adopted the Manning-Oosawa (MO) condensation theory [19, 66] to estimate ξ . In our case, ξ is renormalized to a value 1/4, due to the condensation of tetravalent counterions, while $C_s \geq C_s^* \equiv C_m/4$. For small salt concentration $C_s < C_s^*$, all the tetravalent counterions are expected to condense on the chain, but the number of these ions is not sufficient to renormalize ξ to 1/4. At this moment, ξ decreases linearly from 1 to 1/4 with C_s , or equivalently, $\xi = 1 - 3C_s/C_m$. Plugging ξ and $\kappa^2 = 4\pi\lambda_B(C_m + 4C_s + 4^2C_s)$ into Eq. (9), we obtained ℓ_e^{OSF} , and then, added it to $\ell_{p,0} = 2k_a\langle b \rangle/(k_B T)$ to get the persistence length ℓ_p . Finally, using Eq. (8), we calculated $\langle R_e^2 \rangle^{1/2}$ and the results for different chain stiffness are plotted in dashed curves in Fig. 4. We observed

that the WLC model, combining with the OSF and the MO theories, gives a qualitative prediction for $\langle R_e^2 \rangle^{1/2}$ at low salt concentration for semiflexible and stiff chains. Surprisingly, it also gives a not-bad description of $\langle R_e^2 \rangle^{1/2}$ for the flexible chain with zero k_a and even captures the decreasing behavior up to $C_s = C_s^*$, although the OSF and the MO theories are not expected to work well neither for flexible chains nor for a solution with multivalent salt. The theoretical value is found to be smaller than the value obtained from the simulations. This deviation can be attributed to the effect of the excluded volume interaction, which is neglected in the derivation of the WLC model and should give a positive contribution to the chain size if it is taken into account. In the mid-salt regime, the theory fails to predict $\langle R_e^2 \rangle^{1/2}$ for semiflexible chains. In this region, the chain is condensed by tetravalent counterions. The small chain size suggests that the persistence length is significantly reduced, and as a consequence, the electrostatic persistence length takes a negative value. The negative electrostatic persistence length has been experimentally observed [67]. At high salt concentration, the WLC model again describes well the end-to-end distance except for the case with zero k_a ; at this moment, ℓ_e^{OSF} is almost zero and the persistence length is dominated by the bare persistence length.

D. Snapshots of simulation

Before processing a more quantitative analysis, we present in this section snapshots of our simulations to give readers a vital illustration how the chain looks like in different regions of salt concentration and chain stiffness.

Fig. 5 shows snapshots of a flexible chain at low, middle, and high salt concentrations. The morphology of the chain is elongated at low salt concentration, and displays large-angle turns near the places where the counterions condense, as shown in Fig. 5(a). In the mid-salt region around the equivalence point, the chain collapses and exhibits a randomly-arranged compact structure (see Fig. 5(b)). At high salt concentration (Fig. 5(c)), the chain swells and acquires a zigzagged, extended structure, but not as elongated as at low salt concentration.

Fig. 6 shows snapshots of a semiflexible chain at three salt concentrations. The shape of the chain is smoother than that of the flexible chain. At low salt concentration (Fig. 6(a)), the chain is elongated and not zigzagged. At middle salt concentration, the chain is condensed, and noticeably, forms ordered structure, in contrast to the disordered globule formed

by a flexible chain. Typical ordered structures are shown in Fig. 6(b). They are, from left to right, hairpin, racquet, and toroid. These typical structures have been observed in the experiments of DNA condensation [7, 54, 55, 56]. Unlike the case for flexible chains, a condensed counterion can hardly induce a large-angle turn on the chain backbone. If it is the case, the turn happens to be the folded end of a hairpin structure and counterions are condensed between the two branches of the hairpin. The whole structure looks similar to peas in a pod. At high salt concentration, the chain displays again an elongated structure (see Fig. 6(c)).

Fig. 7 shows the snapshot of a rigid chain. The chain exhibits a stretched structure no matter how many salts are added into the solution. The chain is stiff enough to resist from bending or twisting.

From these snapshots, we found that a compact chain structure is formed when condensed tetravalent counterions can overcome the chain stiffness to bridge between monomers and have enough number to tightly bind the whole chain structure. We observed that, regardless of the chain stiffness, the number of tetravalent counterions condensed on a chain increases with C_s . When C_s is smaller than the equivalence point C_s^* , almost all the tetravalent counterions are condensed on the chain. Only when $C_s > C_s^*$, non-condensed tetravalent counterions can appear in the bulk solution. Moreover, the number of condensed tetravalent counterions surpasses the number needed to neutralize the bare chain charge when $C_s > C_s^*$, and as a consequence, the chain is *locally overcharged* [77]. For flexible chains, there are mainly two effects to drive chain reentrance at high salt concentration. The first one is the Coulomb repulsion between condensed tetravalent counterions. Since the chain is surcharged by the condensed tetravalent counterions, the net repulsion between these ions manifests its effect in the swelling of the chain size. The second one is the presence of the non-condensed tetravalent counterions in the bulk solution. These non-condensed counterions interact with the chain, and can dynamically replace previously condensed counterions and become newly condensed counterions. During this process, the chain morphology oscillates from a loose globule to an expanded structure and vice versa. Increasing salt concentration increases the concentration of non-condensed tetravalent counterions in the bulk, which makes easier the replacement of tetravalent counterions to take place. The chain hence more frequently stays in an expanded state and the averaged chain size increases. For semiflexible chains, there is, in addition, a third effect taking part in the reentrant transition

— the chain stiffness. The chain stiffness always gives an effect against the formation of a compact structure. Together with the instability induced by the presence of non-condensed tetravalent counterions, a chain can dramatically leave a condensed state to an elongated structure at high salt concentration.

E. Probability density distribution

In the previous sections, the conformation of a polyelectrolyte was studied by averaged quantities, such as the root-mean-square R_g and the root-mean-square R_e . In fact, averaged quantities cannot reflect precisely the chain shape since chain morphology varies with time during simulations. In order to understand the details of chain morphology, we investigate in this section the probability density distribution (PDD) of conformational quantities.

Two quantities are studied: The first one is the asphericity A and the second is the radius of gyration R_g . The asphericity A measures the deformation of chain morphology from a spherical geometry and is defined by [68]

$$A = \frac{(\lambda_1 - \lambda_2)^2 + (\lambda_2 - \lambda_3)^2 + (\lambda_3 - \lambda_1)^2}{2(\lambda_1 + \lambda_2 + \lambda_3)^2}. \quad (10)$$

λ_1 , λ_2 , and λ_3 are the three eigenvalues of the gyration tensor of the chain calculated by

$$\mathcal{T}_{\alpha\beta} = \frac{1}{N} \sum_{i=1}^N (\vec{r}_i - \vec{r}_{cm})_{\alpha} (\vec{r}_i - \vec{r}_{cm})_{\beta} \quad (11)$$

where the subfixes α and β denote the three Cartesian components x , y and z . The value of A ranges between 0 and 1. It is equal to 0 for a perfect sphere, 0.25 for a perfect ring, and 1 for a straight line. For a coil chain, $\langle A \rangle$ is 0.431 obtained from simulation [69].

In Fig. 8, parts (a) and (b), we present PDD of asphericity, $p(A)$, and PDD of radius of gyration, $p(R_g)$, for the flexible chain with null k_a . We observed that $p(A)$ shows a peak near $A = 0.8$ in the salt-free solution, indicating that the chain favors an extended structure. The peak gradually moves toward a small A as C_s is increased, and the width of the peak becomes broader. The width then decreases while C_s approaches to the equivalence point C_s^* (Case VI in the figure). At C_s^* , $p(A)$ shows the most pronounced peak at $A \simeq 0.1$, and therefore, the favored morphology is a compact sphere-like structure. If C_s is further increased, the peak becomes broaden and the position of the peak shifts not much toward a larger value. In this salt region, the chain behaves like a random coil and alternates between

a globule and an extended structure. For $p(R_g)$, similar behavior was observed. The peak of $p(R_g)$ moves left to a small R_g and then moves slightly right as C_s is increased. Also, the most pronounced peak appears at the turning point $C_s = C_s^*$.

Figs. 9(a) and (b) shows, respectively, $p(A)$ and $p(R_g)$ for the semiflexible chain with $k_a = 8k_B T / rad^2$. In the low-salt region, $p(A)$ displays a single peak at $A \simeq 0.9$, and therefore, the chain favors to exhibit a rod-like structure. If the salt concentration is increased to some intermediate value, a second peak appears at $A \simeq 0.25$. It indicates the formation of a ring-like (toroid) structure. The second peaks first increases in its height with C_s and then decreases. It disappears while C_s surpasses some critical value, and the chain reattains a rod-like structure. More information can be obtained if we study $p(R_g)$ at the same moment. For example, at $C_s = 2.67 \times 10^{-5} \sigma^{-3}$ (Case III in the figure), $p(R_g)$ shows a doubly peaked distribution and the second peak is roughly situated at the middle position between the first peak and $R_g = 0$. We know from $p(A)$ that the chain exhibits a rod-like structure at this salt concentration. The second peak in $p(R_g)$, hence, corresponds to hairpin structure because hairpin is a two-folded rod and its radius of gyration is equal to half of that of the unfolded rod. Consequently, the chain morphology alternates between unfolded rod and hairpin structure. At higher salt concentration, the first peak in $p(R_g)$ disappears and a new peak appears at $R_g \simeq 5\sigma$. This new peak is attributed to toroidal structure because it corresponds to the peak of $p(A)$ at $A \simeq 0.25$, which is the typical value for a ring structure. Therefore, in this salt region coexist two condensed structures, hairpin and toroid. We noted that probability density for A or R_g is nearly zero between the two peaks when C_s is not large, which indirectly indicates that the structural transition between hairpin and toroid rarely happens during a run. If C_s is large, for instance, $C_s = 6.4 \times 10^{-4} \sigma^{-3}$, a finite value appears between the two peaks, indicating that the two structures can frequently transit between each other. We mention that these results were obtained by doing statistics combined from several independent runs starting with different initial configurations to circumvent the problem of slow transition. At $C_s = 0.00128 \sigma^{-3}$ (Case X in the figure), $p(R_g)$ shows three peaks, indicating a coexistence between the two condensed and the extended-chain structures. One thing is worth to be noticed: In this middle salt region, the peak in $p(R_g)$, which corresponds to a toroidal structure, shifts toward a large value as C_s is increased. It suggests that the toroidal size grows up with salt concentration. This phenomenon is in agreement with the observation of Conwell *et al.* [70]. In the experiment, they found

that monovalent or divalent salt causes an increase in diameter of a condensed DNA toroid. Finally, if C_s goes even higher, $p(R_g)$ displays only one peak at $R_g \simeq 13\sigma$, and hence, the favored shape is an unfolded chain.

We emphasize that the PDDs for the semiflexible chain shows different behavior, compared with the ones for the flexible chain. In the middle salt region, they are multiply peaked and the peaks appear or disappear in a sudden way. Moreover, each peak corresponds to an ordered structure such as toroid or hairpin. On the other hand, the PDDs for the flexible chain display only single peaks and the peak position moves continuously in the space with salt concentration. As a consequence, the coil-globule transition for the semiflexible chain occurs in a discrete manner, whereas in a continuous way for the flexible chain. Both the discrete and the continuous transition have been demonstrated in simulations by other authors [10, 12, 13, 46]. However, the subjects were focused on the chain collapsing from a coil state to a globule state, happened at low salt concentration or at low temperature. Our study presented here goes further and gives a thorough description of how the PDDs varies with salt concentration, not only in the low salt region but also in the high salt region. The sudden appearance and disappearance of peaks show that the discrete nature of transition takes place also at high salt concentration when a semiflexible chain redissolves from an ordered globule state to a coil state. To our knowledge, this is the first time such observation at high C_s is reported.

We present in Fig. 10(a) and Fig. 10(b) $p(A)$ and $p(R_g)$, respectively, for a rigid chain with $k_a = 100k_B T / rad^2$. $p(A)$ shows a sharp peak near $A = 1$ and $p(R_g)$ a sharp peak at R_g around 15σ for all the salt concentration investigated. The chain exhibits a fully extended structure. The results can be verified by estimating the chain length from the radius of gyration. It is known that the length ℓ of a rod is related to the radius of gyration by $R_g^2 = \ell^2 / 12$. Consequently, $R_g = 15\sigma$ yields ℓ equal to 51.96σ , which is in good agreement with the length of a fully extended chain since our chain has 47 bonds and the average bond length is 1.1σ .

We remark that the results presented here were obtained from long simulations. We have calculated the correlation time for the quantities A and R_g at each salt concentration. The results shows that our simulations contains hundreds to thousands independent data for the cases of flexible chain and rigid chain. Therefore, we are confident that Fig. 8 and Fig. 10 report correct equilibrium populations. For the case of semiflexible chain, particularly in

the mid-salt region, the system shows rich morphologies and the transition between different morphologies is slow. We have performed several independent runs to sample different trajectories in order to improve the statistics. The analysis of the correlation time shows that at least, thirty independent samples were cumulated in the simulations. The results reported in Fig. 9, hence, may not be very accurate. However, the PDDs show consistent trend of variation against C_s , and also in Fig. 1, no remarkably large fluctuation is appeared in the $\langle R_g^2 \rangle^{1/2}$ curve. Therefore, these results still give an appreciable description of the equilibrium populations.

F. Dynamics of conformation

We have shown that a polyelectrolyte can be condensed by multivalent salt. Particularly, when the chain is semiflexible, the condensed chain displays an ordered structure, such as hairpin or toroid. In order to get insight of the phenomena, we take the semiflexible chain of $k_a = 8k_B T / rad^2$ as an example, and study in this section how the conformational quantities, A , R_g and R_e , evolve with time.

We focus at first the conformational dynamics at $C_s = 8 \times 10^{-5} \sigma^{-3}$. In Fig. 9, we have demonstrated that the PDDs of the semiflexible chain are doubly peaked at this salt concentration. The chain stays in a hairpin state or a toroid state and the transition between the two states is not frequent. For this case, several independent runs were performed starting with different initial configurations. In order to get insight of the dynamics, we show firstly in Fig. 11 the time evolution of A , R_g and R_e for one of the independent runs, in which the chain exhibits hairpin structure.

The asphericity A fluctuates steadily around 0.9 as shown in Fig. 11(a). At the same moment, the radius of gyration fluctuates around $R_g = 6.5\sigma$ and R_e fluctuates around a small value (see Fig. 11(b)). Therefore, the chain has its two ends fluctuating near the open end of the hairpin structure. Readers can see from the figures that this structure is lasted for a duration of at least 2×10^8 simulation steps in this run. Please be aware that 2×10^8 simulation steps is a long time period in a typical molecular simulation. In our case, it is approximately equal to a duration of $2\mu s$, provided that σ is 2.4\AA , T is 300K and m is 200Da.

We then show in Fig. 12 the dynamics of these quantities when the chain exhibits toroidal

structure. The asphericity A fluctuates around 0.25 except at four places, fluctuating around 0.7 (cf. Fig. 12(a)). At these four places, the chain displays a twisted ring structure, similar to the shape of the digit ‘8’. Since the two ends of a toroidal chain is generally not very close to each other, R_e fluctuates around a large value (see Fig. 12(b)), compared to the value for hairpin structure (Fig. 11(b)). Resembling the previous run, the toroid structure is continued for nearly 2×10^8 simulation steps. The morphological transition between toroid and hairpin is, hence, not frequent at this salt concentration.

The transition between different ordered structures becomes observable in simulations if the salt concentration is high. For example, at $C_s = 6.4 \times 10^{-4} \sigma^{-3}$ (shown in Fig. 13(a)), the asphericity fluctuates around two values, at $A = 0.25$ and at $A = 0.85$, which indicates the transition between ring-like and rod-like structures. Moreover, Fig. 13(b) shows that the radius of gyration associated to the rod-like structure is larger than that associated to the ring-like structure, but the end-to-end distance is smaller. It enables us to identify this rod-like structure to be a two-folded chain (*i.e.* hairpin), which was also confirmed from the simulation snapshots. The second example is chosen at $C_s = 1.28 \times 10^{-3} \sigma^{-3}$ (see Fig. 14). The asphericity shows similar fluctuation around the two values. However, the value, $A \simeq 0.85$, which corresponds to rod-like structure, is now associated to two behaviors of R_g , fluctuating at $R_g \simeq 6.5\sigma$ and $R_g \simeq 13\sigma$. Combining the information obtained from R_e , we assert that the first fluctuation of R_g corresponds to a two-folded chain structure and the second one corresponds to an unfolded-chain structure. Therefore, the chain transits between three states, which are unfolded chain state, hairpin state, and toroid state.

Recently, dynamic exchange between toroid and folded-chain structures in a salt-free solution of semiflexible polyelectrolyte has been numerically demonstrated by tuning the Coulomb strength parameter [11]. The work showed a back-and-forth flipping between the two structures, similar to our observations. Our study, moreover, showed that transitions between different chain states can be enhanced by addition of multivalent salt beyond the equivalence point C_s^* . The mechanism is understood as follows. Below C_s^* , most of the multivalent counterions are condensed on the chain. Roughly while C_s is larger than C_s^* , multivalent counterions start to exist in the bulk solution. Therefore, increasing salt concentration increases the number of the multivalent counterions surrounding but not condensed on the chain. Due to the presence of these surrounding counterions, the chance for a chain to escape from its current condensed state is increased. The surrounding multivalent counteri-

ons strongly interact with the chain, and can induce local change of the chain morphology by the replacing process: some of the condensed ions on the chain are released into the solution and replaced with the surrounding ions. Occasionally, the chain forms a newly condensed structure.

G. Schematic State diagram

The conformation of our single polyelectrolytes, classified by the three categories: *flexible* chain, *semiflexible* chain, and *rigid* chain, is summarized in a schematic state diagram shown in Fig. 15.

Flexible chain exhibits an extended structure in a salt-free solution, and continuously collapse to a compact, spherical structure as C_s is increased to the equivalence point. Further increasing C_s gradually leads chain discondensation. At very high salt concentration, the chain behaves similar to a random coil.

Semiflexible chain shows different conformations as multivalent salt is added into the solution. At very low salt concentration, the chain exhibits an elongated structure. If C_s is increased beyond the first critical value C_c , the chain bends over upon itself and forms two-folded rod structure (hairpin). This structure is not so stable that the chain morphology alters between a hairpin and an extended structure. Further increasing C_s firstly stabilizes the hairpin structure, and eventually, leads to the appearance of toroidal structure. At this moment, hairpin and toroid structures coexist in the solution. We found that the rate of transition between hairpin and toroid increases with the salt concentration. Therefore, the transition becomes observable during limited time period of a molecular simulation while C_s is large enough. If C_s is not large enough, the two structures can be observed only in independent runs, since our model system contains solely one chain. The formation of these ordered structures has been proposed to be a consequence of a nucleation-growth process derived from the thermal fluctuations in chain morphology [71, 72, 73]. At higher salt concentration, the chain can even transit between three morphological states: the unfolded-rod state, the hairpin state, and the toroid state. Finally, if C_s surpasses the second critical value C_d , the chain can no longer be collapsed, and consequently, reattains a unfolded, rod-like structure.

Rigid chain, just as its name denotes, is rigid, no matter how many salts are added in

the solution, and always shows a rodlike, fully stretched structure in simulations.

The state diagram presented here is in accordance with the results obtained by other authors, although the employed models are different. For example, Ou and Muthukumar investigated the conformation of single polyelectrolytes in a salt-free solution and the chains were collapsed by increasing Coulomb strength parameter Γ [11]. They observed that a semiflexible chain stays, in turn, in a coil state, a folded-rod state, and a toroid state, as Γ is increased (cf. Fig. 6 of Ref. [11]). The result is consistent with what we observed in the region where chains are collapsed. For the second example, we mention the works done by Ivanov and his coworkers [13, 61]. In their works, the effects of chain stiffness and chain length on the conformation of neutral polymers were studied. They found that finite chain length can make unsharpened the coil-to-toroid transition driven by temperature reduction, and several intermediate states, such as folded-rod and disk-like structures, were observed in the transition region. The proposed state diagram is in analogy of our results in the low-salt region. We remark that chain length is an important factor in determination of the chain morphology. Experiments have shown that short DNA molecules are more easily condensed to folded rods than toroids [2, 57, 58]. This phenomenon gives an explanation of why the hairpin structure appears frequently in our state diagram. It is because the modeled chain is not long in our study. Nonetheless, the schematic state diagram obtained here has gone beyond the works done by other authors. We investigated the salt-induced conformation of polyelectrolytes thoroughly in a *direct* way since this topic has attracted much attention in scientific community [74, 75], and explored the situations from a salt-free condition to a very high salt concentration so that chain condensation and redissolution are both occurred. The findings give deep insight of the phenomena of DNA condensation at molecular level and are relevant for a broad range of salt-induced complexation phenomena.

IV. CONCLUSION

We have performed Langevin dynamics simulations to study single polyelectrolytes in tetravalent salt solutions under the framework of a coarse-grained model. The effect of salt concentration and the role of chain stiffness on the properties of chain conformation have been discussed. In order to understand thoroughly the reentrant condensation, a broad range of salt concentration has been investigated so that the single polyelectrolytes display,

in turn, collapsing transition and swelling transition upon addition of salt.

We have observed that chain morphology crucially depends on chain stiffness. At a fixed chain length, the radius of gyration R_g of a polyelectrolyte varies in three different ways with the salt concentration C_s . Based upon these variations, we can classify polyelectrolytes into three categories. The first category is *flexible* chain for which $\langle R_g^2 \rangle^{1/2}$ shows a tilted L-shaped curve as a function of C_s in the semilog plot. The second one is *semiflexible* chain which is characterized by an U-shaped $\langle R_g^2 \rangle^{1/2}$ curve. And the third one is *rigid* chain for which $\langle R_g^2 \rangle^{1/2}$ is roughly a constant, no matter how many salts are added in the solution. The end-to-end distance shows the similar variation as the radius of gyration. However, its value does not always reflect the real chain size, particularly when the chain is condensed to an orderly packed structure such as hairpin. Moreover, we have found that the WLC model with persistence length obtained by the OSF theory qualitatively predicts the end-to-end distance at low and at high salt concentrations for semiflexible and rigid chains. Surprisingly, these theories also give a not-bad description of the decreasing behavior of $\langle R_e^2 \rangle^{1/2}$ against C_s for flexible chain up to $C_s = C_s^*$, although they are not expected to work well neither for flexible chains nor for a solution with multivalent salt.

We have found that in a salt-free or vary low-salt solution, the degree of swelling of a polyelectrolyte decreases with increasing the chain stiffness, in reference of the size of the uncharged counterpart of the chain. On the other hand, in a high-salt region, it tends toward zero, regardless of the chain stiffness. As a consequence, at high C_s , a semiflexible chain reattains a dimension close to the chain size in the absence of salt, but not does a flexible one. We have discussed the reasons for the occurrence of chain reentrance or swelling at high salt concentration. For flexible chains, two effects can possibly drive this phenomenon: (1) the net Coulomb repulsion between condensed multivalent counterions which locally overcharges the chain, (2) the instability derived from the presence of non-condensed multivalent counterions in a bulk solution. For semiflexible chains, the chain stiffness plays, in addition, the imperative role on reexpanding the chain.

The chain stiffness has been witnessed to influence both the local and the global structures of a polyelectrolyte. A flexible chain shows a zigzagged local structure in the presence of multivalent salt and the condensed structure is disordered. In contrast, a semiflexible chain locally shows smooth morphology. Large-angle turn on the chain backbone can only be observed when the chain is condensed to a hairpin structure. Moreover, the global structure

of a condensed chain is orderly packed. Hairpin and toroid are the two favored structures.

The chain stiffness affects also the nature of the structural transition. By studying the probability density distributions of asphericity A and of R_g , we have demonstrated that a semiflexible chain undergoes a coil-globule transition in a discrete manner between an extended structure and a condensed, ordered structure, whereas a flexible chain undergoes a continuous transition. This discrete nature is happened not only in the low-salt region when chain condensation occurs, but also in the high-salt region when chain reenters into the solution.

We have studied the dynamics of the conformational quantities of a semiflexible chain. Upon addition of salt beyond the first critical concentration C_c , the chain is folded to a hairpin structure. However, it is a dynamic equilibrium process and the chain morphology alters between a hairpin and a unfolded-chain structure. Further increasing C_s firstly stabilizes the hairpin structure and then triggers the birth of toroid structure. Transition between hairpin and toroid becomes more frequent as C_s getting higher. When C_s approaches the second critical concentration C_d , these two structures become unstable and the chain can stay again in a unfolded state, coexisting with the two condensed structures. At the end, we summarized the conformation of individual polyelectrolytes in a state diagram. Although the modeled chain is not very long, our results agree with experiments and other numerical works in many aspects in the chain condensation region. The work presented here goes further to investigate in detail the microstructure and the dynamics of a chain in the chain redissolution region, which gives us a thorough vision of the behavior of polyelectrolytes in salt solutions. Since chain length is also a relevant factor to affect the morphology of a chain, it will be very interesting to study the effect of finite chain length. That will be the topic of our future work.

V. ACKNOWLEDGMENTS

This material is based upon work supported by the National Science Council, the Republic of China, under the contract No. NSC 95-2112-M-007-025-MY2. A large part of the simulations was run using the resources of the National Center for High-performance Computing under the project “Taiwan Knowledge Innovation National Grid”. The authors

express their gratitude to the members and the staffs of the council and the center.

- [1] L. C. Gosule and J. A. Schellman, *Nature* **259**, 333 (1976).
- [2] P. G. Arscott, A.-Z. Li, and V. A. Bloomfield, *Biopolymers* **30**, 619 (1990).
- [3] V. A. Bloomfield, *Curr. Opin. Struct. Biol.* **6**, 334 (1996).
- [4] K. Yoshikawa and Y. Yoshikawa, in *Pharmaceutical Perspectives of Nucleic Acid-Based Therapeutics*, edited by R. I. Mahato and S. W. Kim (Taylor & Francis, London, 2002), pp. 136–163.
- [5] M. Olvera de la Cruz, L. Belloni, M. Delsanti, J. P. Dalbiez, O. Spalla, and M. Drifford, *J. Chem. Phys.* **103**, 5781 (1995).
- [6] E. Raspaud, M. Olvera de la Cruz, J.-L. Sikorav, and F. Livolant, *Biophys. J.* **74**, 381 (1998).
- [7] G. Maurstad, S. Danielsen, and B. T. Stokke, *J. Phys. Chem. B* **107**, 8172 (2003).
- [8] J. Widom and R. L. Baldwin, *J. Mol. Biol.* **144**, 431 (1980).
- [9] G. E. Plum, P. G. Arscott, and V. A. Bloomfield, *Biopolymers* **30**, 631 (1990).
- [10] M. O. Khan and D. Y. C. Chan, *Macromolecules* **38**, 3017 (2005).
- [11] Z. Ou and M. Muthukumar, *J. Chem. Phys.* **123**, 074905 (2005).
- [12] H. Noguchi and K. Yoshikawa, *J. Chem. Phys.* **109**, 5070 (1998).
- [13] V. A. Ivanov, M. R. Stukan, V. Vasilevskaya, W. Paul, and K. Binder, *Macromol. Theory Simul.* **9**, 488 (2000).
- [14] H. R. Kruyt, ed., *Colloid Science*, vol. II (Elsevier Publishing Company, New York, 1949).
- [15] T. T. Nguyen, I. Rouzina, and B. I. Shklovskii, *J. Chem. Phys.* **112**, 2562 (2000).
- [16] H. G. Bungenberg de Jong and J. Lens, *Bioch. Z.* **235**, 185 (1931).
- [17] R. W. Wilson and V. A. Bloomfield, *Biochem.* **18**, 2192 (1979).
- [18] Y. Yamasaki, Y. Teramoto, and K. Yoshikawa, *Biophys. J.* **80**, 2823 (2001).
- [19] F. Oosawa, *Polyelectrolytes* (Marcel Dekker, New York, 1971).
- [20] I. Rouzina and V. A. Bloomfield, *J. Phys. Chem.* **100**, 9977 (1996).
- [21] A. Y. Grosberg, T. T. Nguyen, and B. I. Shklovskii, *Rev. Mod. Phys.* **74**, 329 (2002).
- [22] F. J. Solis and M. Olvera de la Cruz, *J. Chem. Phys.* **112**, 2030 (2000).
- [23] F. J. Solis and M. Olvera de la Cruz, *Eur. Phys. J. E* **4**, 143 (2001).
- [24] F. J. Solis, *J. Chem. Phys.* **117**, 9009 (2002).
- [25] I. M. Lifshitz, A. Y. Grosberg, and A. R. Khokhlov, *Rev. Mod. Phys.* **50**, 683 (1978).

- [26] C. B. Post and B. H. Zimm, *Biopolymers* **21**, 2123 (1982).
- [27] K. Ghosh, G. A. Carri, and M. Muthukumar, *J. Chem. Phys.* **116**, 5299 (2002).
- [28] K. Yoshikawa and Y. Matsuzawa, *Physica D* **84**, 220 (1995).
- [29] K. Yoshikawa, M. Takahashi, V. V. Vasilevskaya, and A. R. Khokhlov, *Phys. Rev. Lett.* **76**, 3029 (1996).
- [30] M. J. Stevens and K. Kremer, *Phys. Rev. Lett.* **71**, 2228 (1993).
- [31] M. J. Stevens and K. Kremer, *J. Chem. Phys.* **103**, 1669 (1995).
- [32] R. G. Winkler, M. Gold, and P. Reineker, *Phys. Rev. Lett.* **80**, 3731 (1998).
- [33] J. C. Chu and C. H. Mak, *J. Chem. Phys.* **110**, 2669 (1999).
- [34] U. Micka, C. Holm, and K. Kremer, *Langmuir* **15**, 4033 (1999).
- [35] M. J. Stevens, *Biophys. J.* **80**, 130 (2001).
- [36] R. Chang and A. Yethiraj, *J. Chem. Phys.* **116**, 5284 (2002).
- [37] S. Liu and M. Muthukumar, *J. Chem. Phys.* **116**, 9975 (2002).
- [38] A. A. C. C. Pais, M. G. Miguel, P. Linse, and B. Lindman, *J. Chem. Phys.* **117**, 1385 (2002).
- [39] M. Deserno, A. Arnold, and C. Holm, *Macromolecules* **36**, 249 (2003).
- [40] H. J. Limbach and C. Holm, *J. Phys. Chem. B* **107**, 8041 (2003).
- [41] M. J. Stevens and S. J. Plimpton, *Eur. Phys. J. B* **2**, 341 (1998).
- [42] M. O. Khan, S. M. Mel'nikov, and B. Jönsson, *Macromolecules* **32**, 8836 (1999).
- [43] M. Deserno, F. Jiménez-Ángeles, C. Holm, and M. Lozada-Cassou, *J. Phys. Chem. B* **105**, 10983 (2001).
- [44] S. Liu, K. Ghosh, and M. Muthukumar, *J. Chem. Phys.* **119**, 1813 (2003).
- [45] R. S. Dias, A. A. C. C. Pais, and M. G. Miguel, *J. Chem. Phys.* **119**, 8150 (2003).
- [46] J. M. G. Sarraguça, M. Skepo, A. A. C. C. Pais, and P. Linse, *J. Chem. Phys.* **119**, 12621 (2003).
- [47] J. Kłos and T. Pakula, *J. Chem. Phys.* **122**, 134908 (2005).
- [48] E. Allahyarov, G. Gompper, and H. Löwen, *J. Phys.: Condens. Matter* **17**, S1827 (2005).
- [49] P.-Y. Hsiao, *J. Chem. Phys.* **124**, 044904 (2006).
- [50] P.-Y. Hsiao, *Macromolecules* **20**, 7125 (2006).
- [51] P.-Y. Hsiao and E. Luijten, *Phys. Rev. Lett.* **97**, 148301 (2006).
- [52] C. L. Ma and V. A. Bloomfield, *Biophys. J.* **67**, 1678 (1994).
- [53] G. Maurstad and B. T. Stokke, *Curr. Opin. Colloid Interface Sci.* **10**, 16 (2005).

- [54] D. K. Chattoraj, L. C. Gosule, and J. A. Schellman, *J. Mol. Biol.* **121**, 327 (1978).
- [55] A. Martin, M. C. Davies, B. J. Rackstraw, C. J. Roberts, S. Stolnik, S. J. B. Tendler, and P. M. Williams, *FEBS Letters* **480**, 106 (2000).
- [56] K. Yoshikawa, Y. Yoshikawa, and T. Kanbe, *Chem. Phys. Lett.* **354**, 354 (2002).
- [57] R. Marquet, A. Wyart, and C. Houssier, *Biochim. Biophys. Acta* **909**, 165 (1987).
- [58] V. A. Bloomfield, *Biopolymers* **31**, 1471 (1991).
- [59] H.-L. Cheng and K.-F. Lin, *Langmuir* **18**, 7287 (2002).
- [60] J. M. G. Sarraguça and A. A. C. C. Pais, *Phys. Chem. Chem. Phys.* **8**, 4233 (2006).
- [61] M. R. Stukan, V. A. Ivanov, A. Y. Grosberg, W. Paul, and K. Binder, *J. Chem. Phys.* **118**, 3392 (2003).
- [62] J. Pelta, F. Livolant, and J.-L. Sikorav, *J. Biol. Chem.* **271**, 5656 (1996).
- [63] M. Rubinstein and R. H. Colby, *Polymer Physics* (Oxford University Press, 2003).
- [64] T. Odijk, *J. Polym. Sci., Polym. Phys. Ed.* **15**, 477 (1977).
- [65] J. Skolnick and M. Fixman, *Macromolecules* **10**, 944 (1977).
- [66] G. S. Manning, *J. Chem. Phys.* **51**, 924 (1969).
- [67] C. G. Baumann, S. B. Smith, V. A. Bloomfield, and C. Bustamante, *Proc. Natl. Acad. Sci. USA* **94**, 6185 (1997).
- [68] J. Rudnick and G. Gaspari, *J. Phys. A: Math. Gen.* **19**, L191 (1986).
- [69] M. Bishop and C. J. Saltiel, *J. Chem. Phys.* **88**, 6594 (1988).
- [70] C. C. Conwell, I. D. Vilfan, and N. V. Hud, *Proc. Natl. Acad. Sci. USA* **100**, 9296 (2003).
- [71] K. Yoshikawa and Y. Matsuzawa, *J. Am. Chem. Soc.* **118**, 929 (1996).
- [72] T. Sakaue and K. Yoshikawa, *J. Chem. Phys.* **117**, 6323 (2002).
- [73] N. V. Hud and I. D. Vilfan, *Annu. Rev. Biophys. Biomol. Struct.* **34**, 259 (2005).
- [74] S. K. Tripathy, J. Kumar, and H. S. Nalwa, eds., *Handbook of Polyelectrolytes and Their Applications*, vol. I, II, III (American Scientific, Stevenson Ranch, CA, 2002).
- [75] M. A. Findeis, ed., *Nonviral Vectors for Gene Therapy: Methods and Protocols* (Humana Press, 2001).
- [76] Refer to web site <http://lammmps.sandia.gov/> for more information about LAMMPS.
- [77] “Locally overcharged” does not necessarily mean a reversal of the sign of the effective chain charge because counterions and coions can form layering organization around a polyelectrolyte at high salt concentration, resulting in an oscillatory charge distribution around a chain. See

Refs [49, 50] for detailed discussions for flexible chains.

Figure captions

FIG 1 $\langle R_g^2 \rangle^{1/2}$ as a function of C_s for the chains of different stiffness k_a .

FIG 2 $\alpha \equiv (\langle R_g^2 \rangle^{1/2} / \langle R_{g,n}^2 \rangle^{1/2}) - 1$ as a function of C_s for the chains of different stiffness k_a .

FIG 3 α as a function of k_a at different salt concentration C_s .

FIG 4 $\langle R_e^2 \rangle^{1/2}$ as a function of C_s for the chains of different k_a . The dashed curves denote the prediction of the WLC model combined with the OSF and MO theories for different values of k_a , indicated on the left-hand side of the corresponding curve.

FIG 5 Snapshots of simulation for a flexible chain ($k_a = 0k_B T / rad^2$) at (a) $C_s = 1.33 \times 10^{-5} \sigma^{-3}$, (b) $C_s = 8 \times 10^{-5} \sigma^{-3}$, and (c) $C_s = 5.12 \times 10^{-3} \sigma^{-3}$. The gray bead-spring chain represents the polyelectrolyte, the black spheres represent the tetravalent counterions, and the white spheres represent the monovalent counterions. Coions are not shown for the reason of clarity.

FIG 6 Snapshots of simulation for a semiflexible chain ($k_a = 8k_B T / rad^2$) at (a) $C_s = 1.33 \times 10^{-5} \sigma^{-3}$, (b) $C_s = 6.4 \times 10^{-4} \sigma^{-3}$, and (c) $C_s = 5.12 \times 10^{-3} \sigma^{-3}$. The gray bead-spring chain represents the polyelectrolyte, the black spheres represent the tetravalent counterions, and the white spheres represent the monovalent counterions. Coions are not shown for the reason of clarity.

FIG 7 Snapshots of simulation for a rigid chain ($k_a = 100k_B T / rad^2$) at $C_s = 8 \times 10^{-5} \sigma^{-3}$. The gray bead-spring chain represents the polyelectrolyte, the black spheres represent the tetravalent counterions, and the white spheres represent the monovalent counterions. Coions are not shown for the reason of clarity.

FIG 8 (a) $p(A)$, and (b) $p(R_g)$ of the flexible chain with zero stiffness for the cases of different C_s . Each case is numbered in Roman number along ‘Case’-axis. The value in the parenthesis following the Roman number denotes the salt concentration in the unit $10^{-5} \sigma^{-3}$.

FIG 9 (a) $p(A)$, and (b) $p(R_g)$ of the semiflexible chain with $k_a = 8k_B T / rad^2$ for the cases of different C_s . Each case is numbered in Roman number along ‘Case’-axis. The value

in the parenthesis following the Roman number denotes the salt concentration in the unit $10^{-5}\sigma^{-3}$.

FIG 10 (a) $p(A)$, and (b) $p(R_g)$ of a rigid chain with $k_a = 100k_BT/rad^2$ for the cases of different C_s . Each case is numbered in Roman number along ‘Case’-axis. The value in the parenthesis following the Roman number denotes the salt concentration in the unit $10^{-5}\sigma^{-3}$.

FIG 11 Time evolution of (a) A , and (b) R_g and R_e , at $C_s = 8 \times 10^{-5}\sigma_m^{-3}$ where the chain exhibits a hairpin structure.

FIG 12 Time evolution of (a) A , and (b) R_g and R_e , at $C_s = 8 \times 10^{-5}\sigma_m^{-3}$ where the chain shows a toroidal structure.

FIG 13 Time evolution of (a) A , and (b) R_g and R_e , at $C_s = 6.4 \times 10^{-4}\sigma_m^{-3}$ where the chain alters between a hairpin and a toroid structure.

FIG 14 Time evolution of (a) A , and (b) R_g and R_e , at $C_s = 1.28 \times 10^{-3}\sigma_m^{-3}$ where the chain morphology alters between a hairpin, a toroid, and an unfolded-chain structure.

FIG 15 Schematic state diagram for our single polyelectrolytes. A double-headed arrow appeared between two states denotes that the structural transition can take place in a typical simulation run at that condition.

Figures 1—15

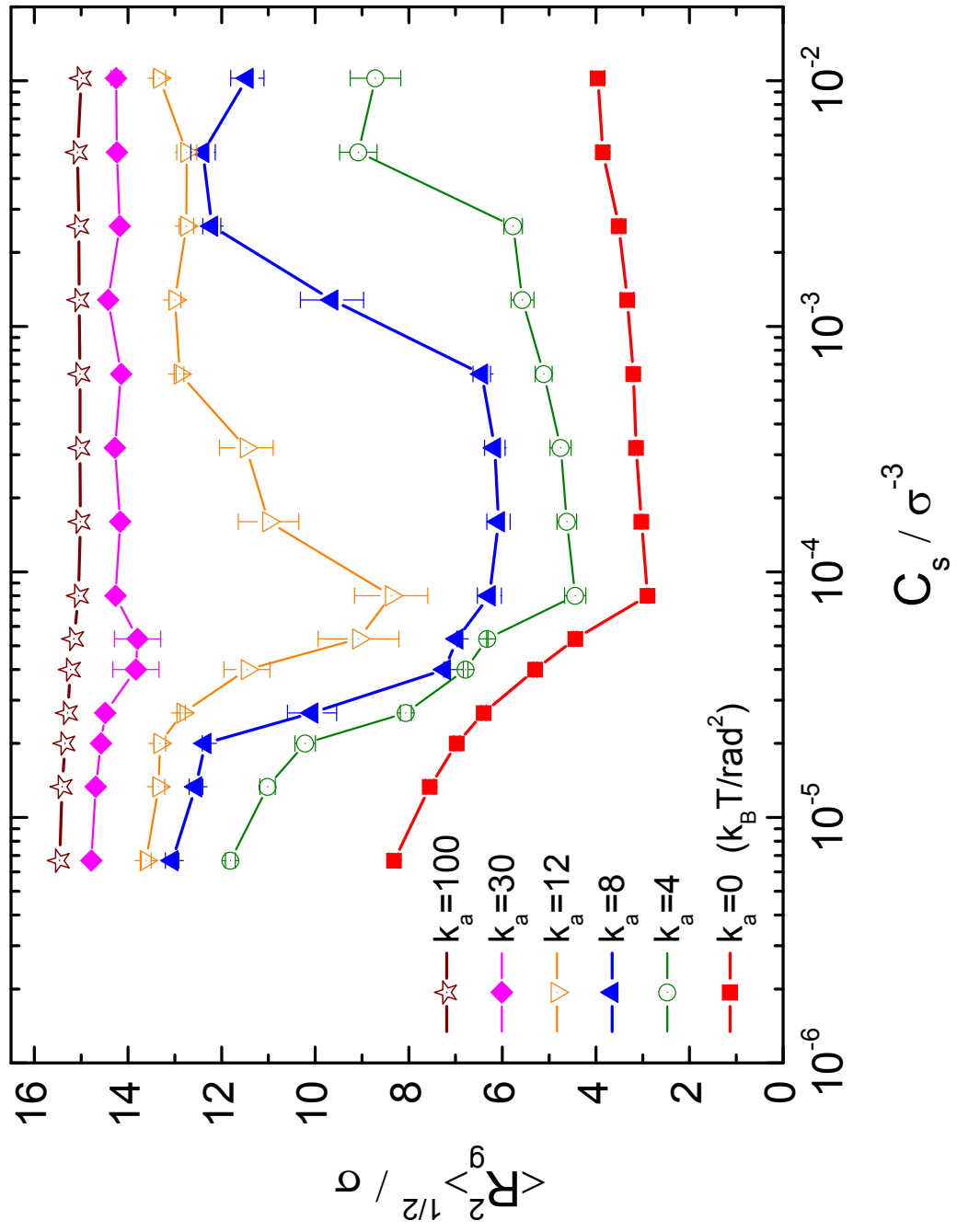


FIG. 1:

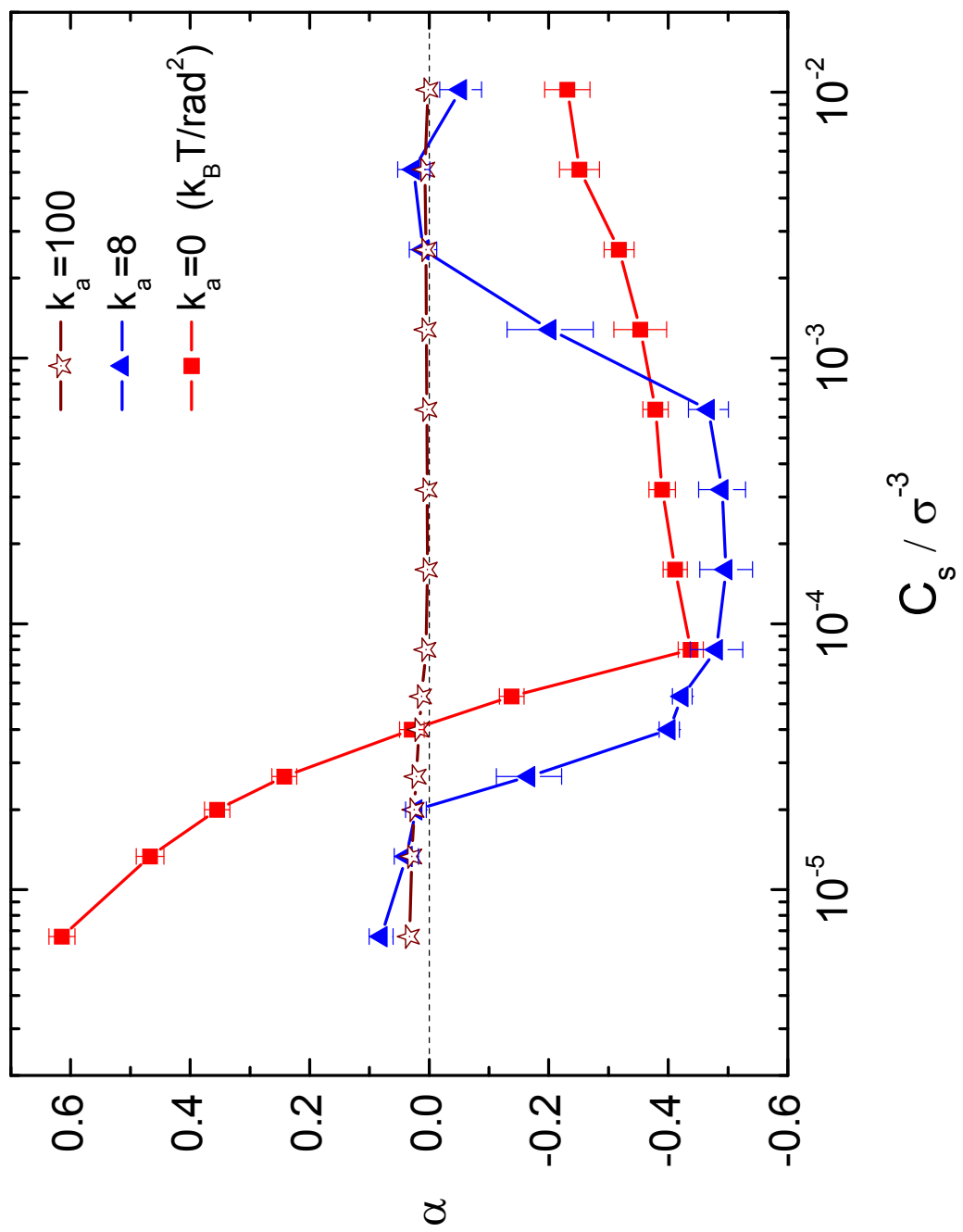


FIG. 2:

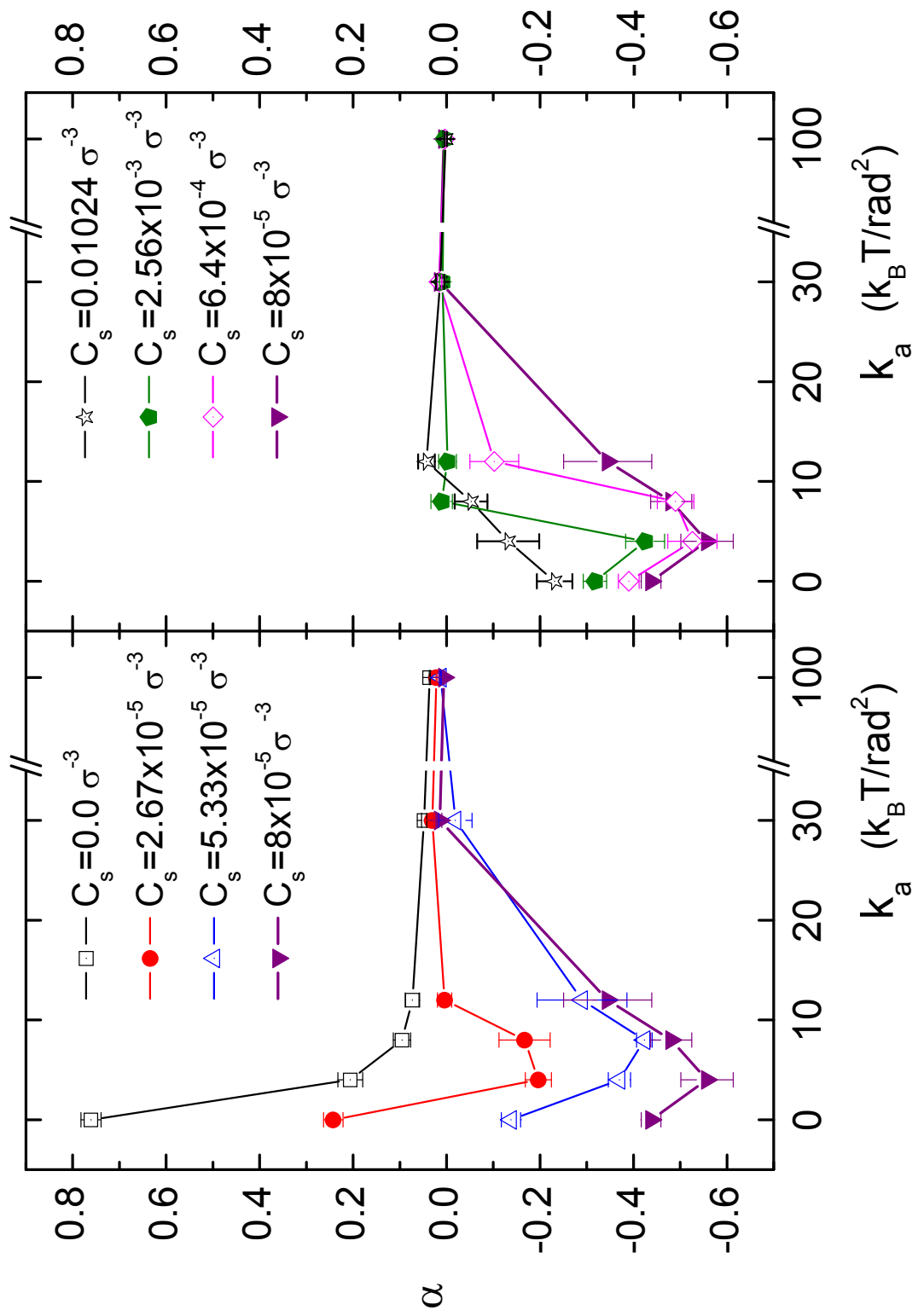


FIG. 3:

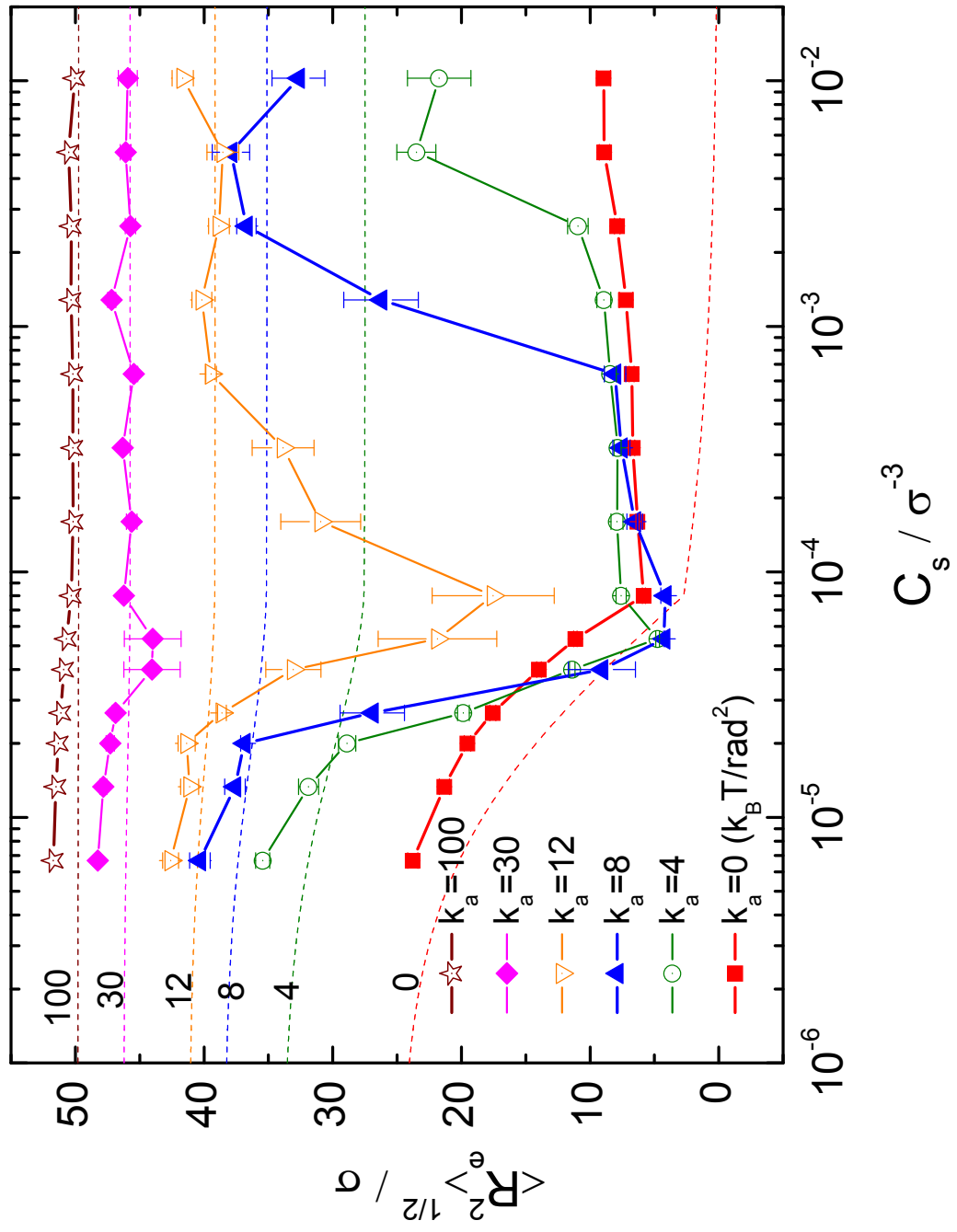
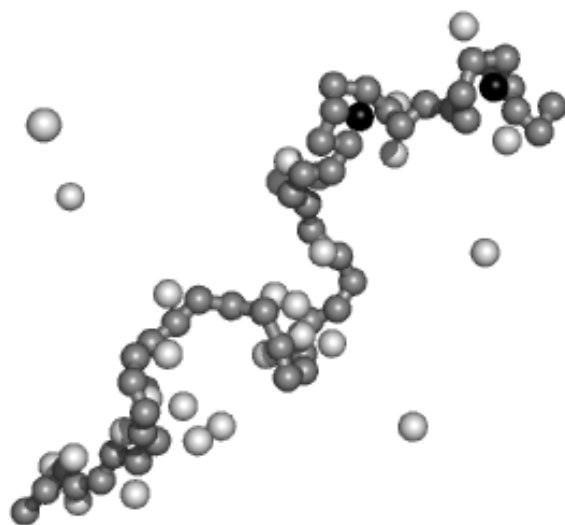
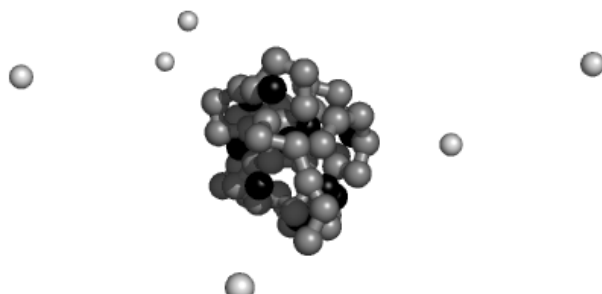


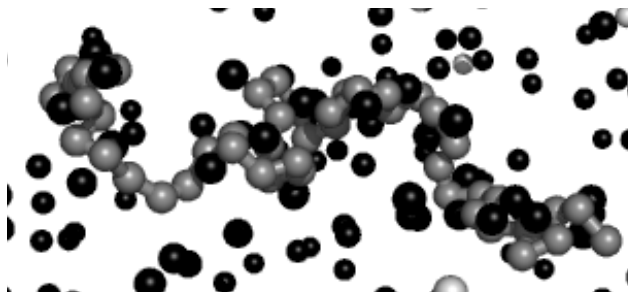
FIG. 4:



(a)

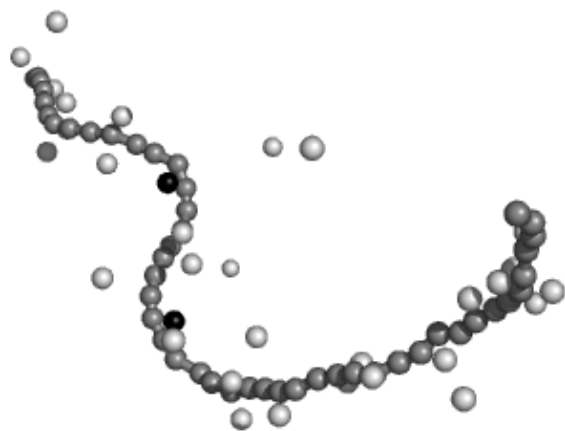


(b)



(c)

FIG. 5:



(a)



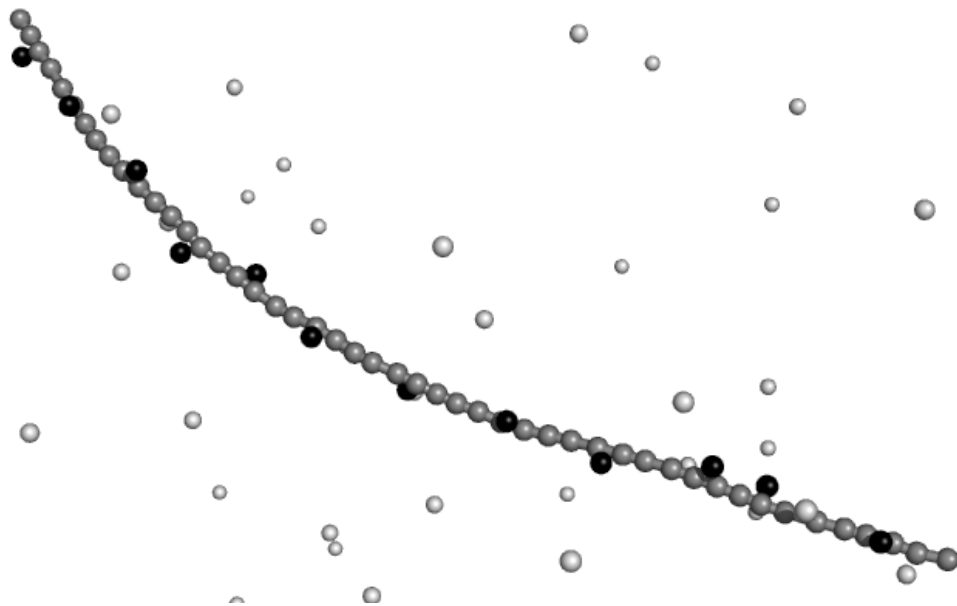


FIG. 7:

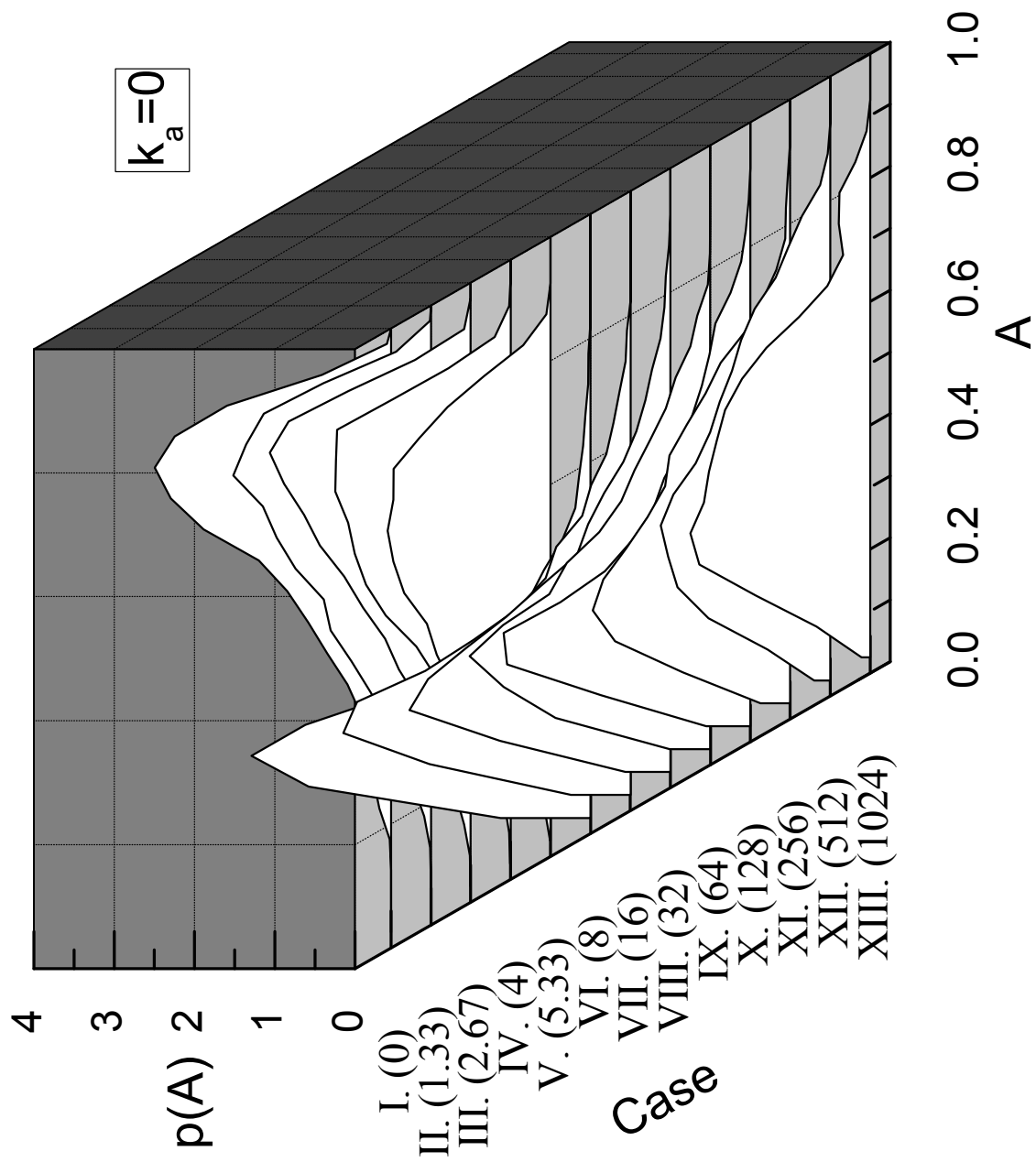


FIG. 8: (a)

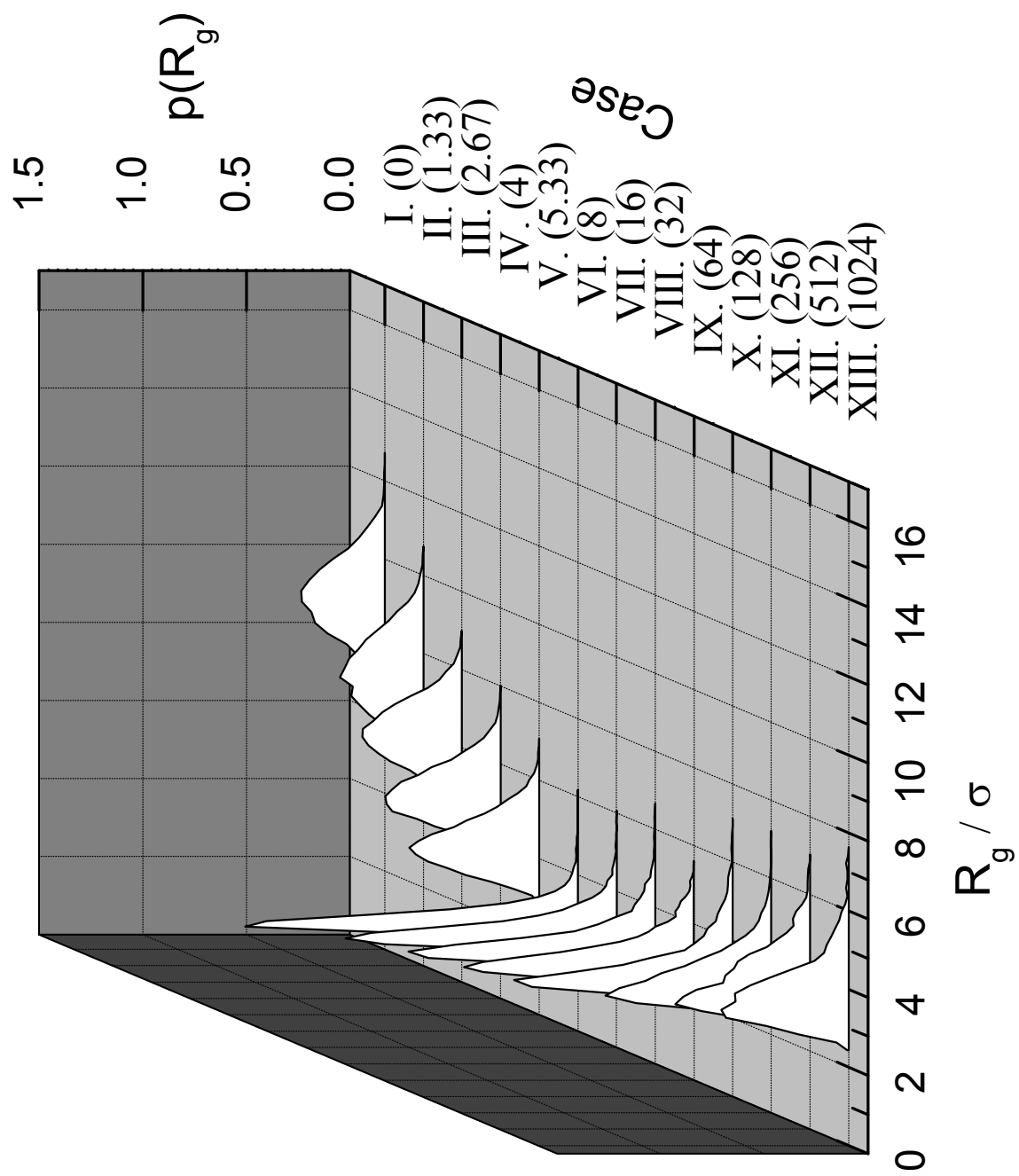


FIG. 8: (b)

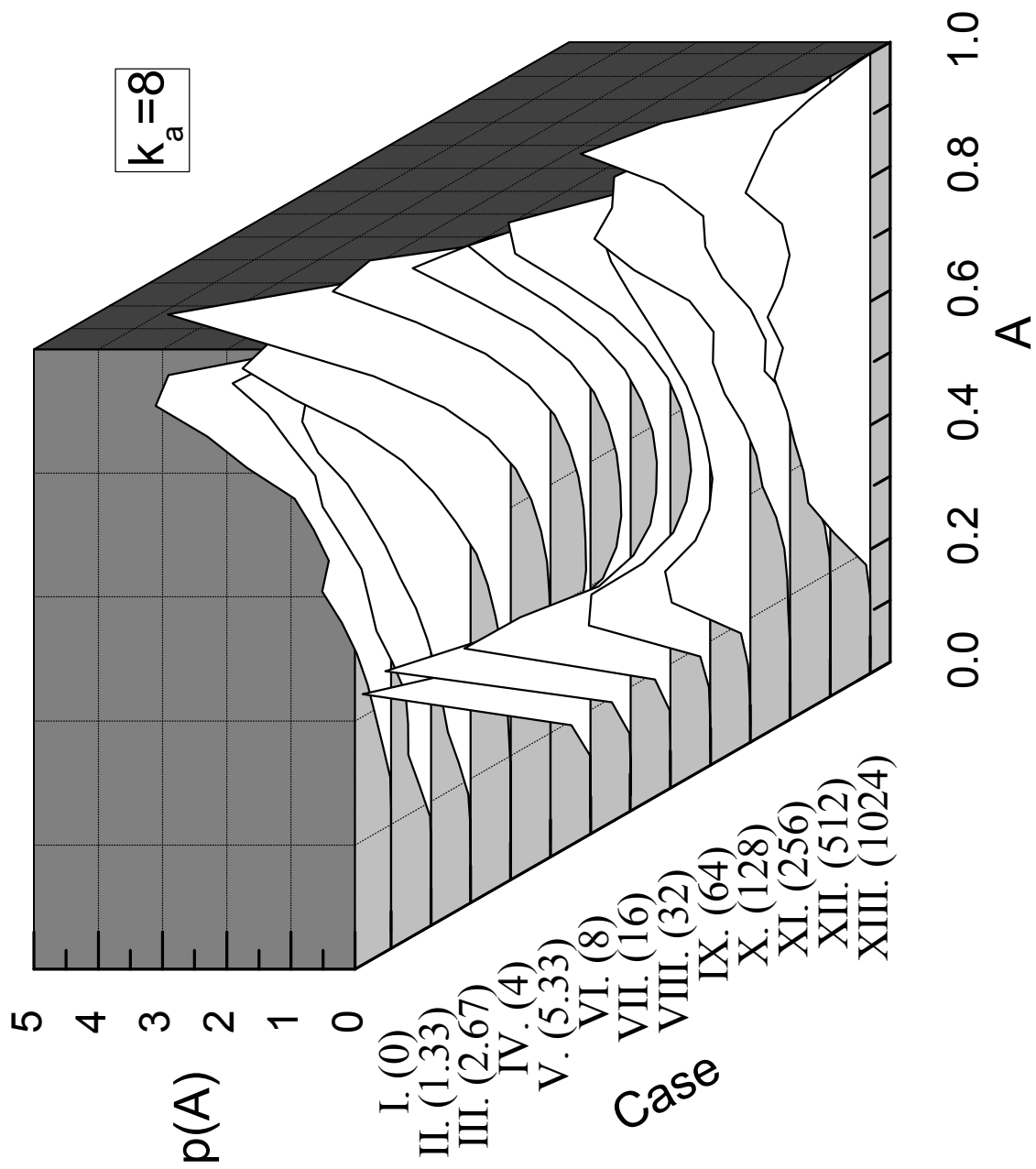


FIG. 9: (a)

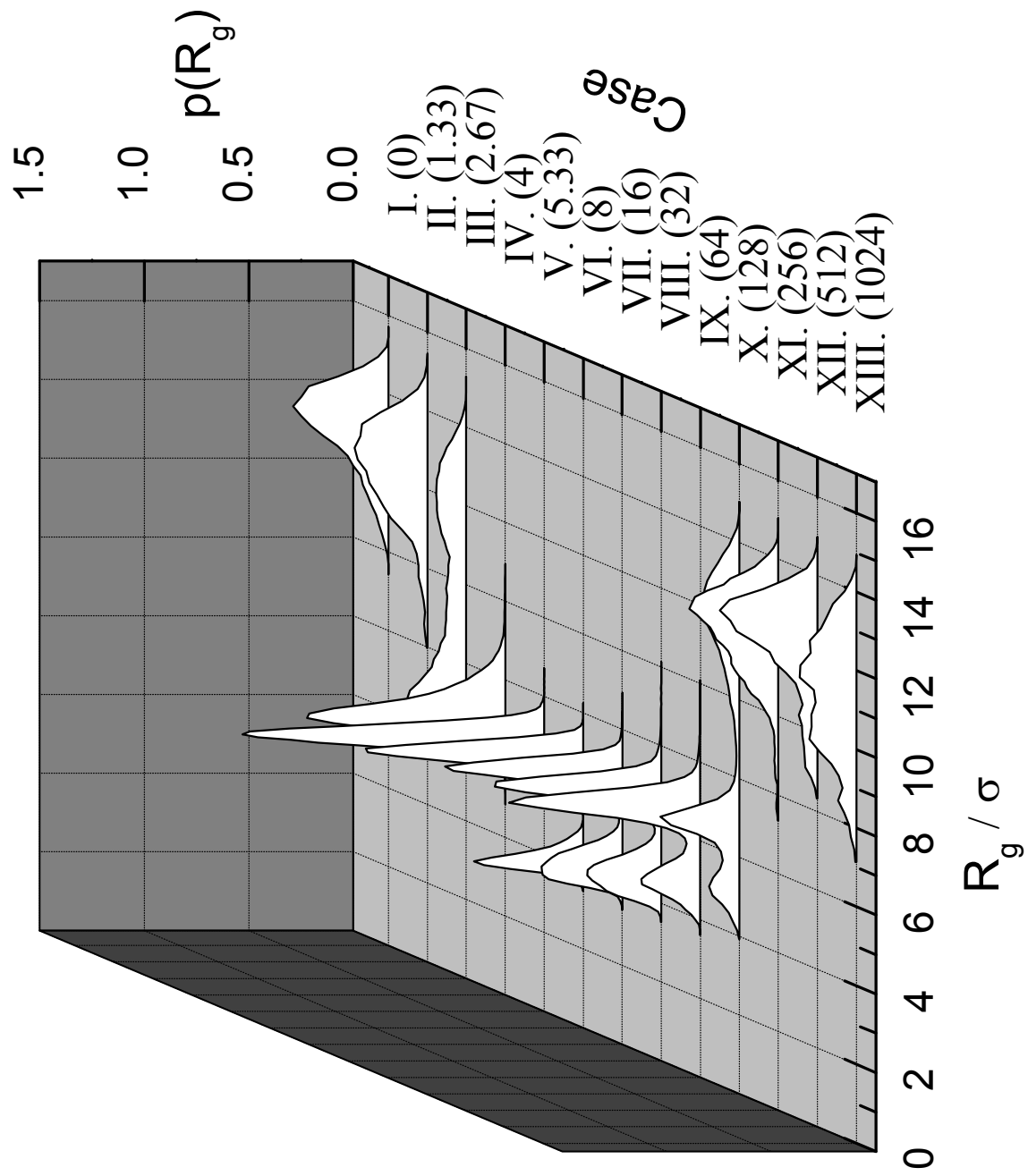


FIG. 9: (b)

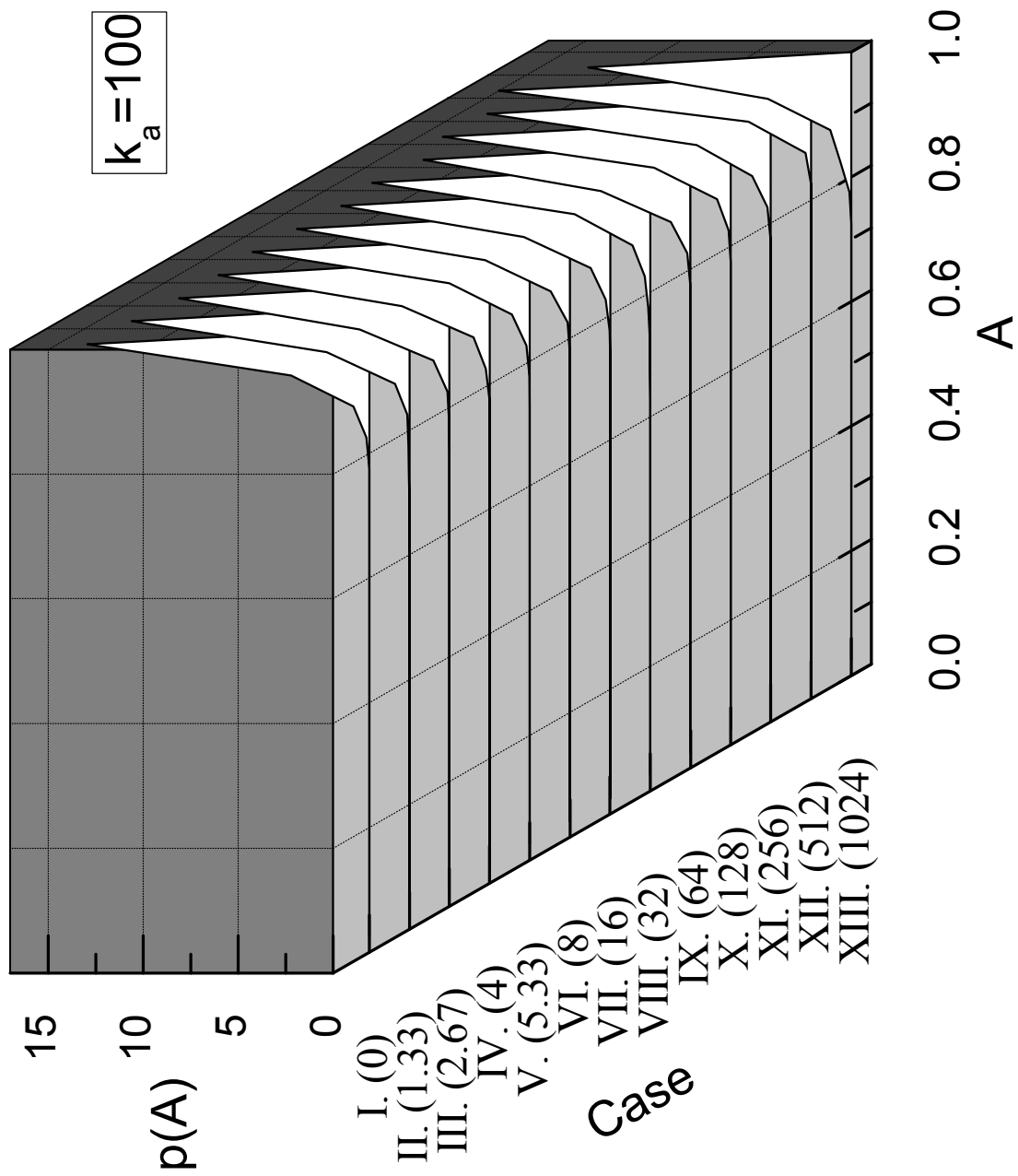


FIG. 10: (a)

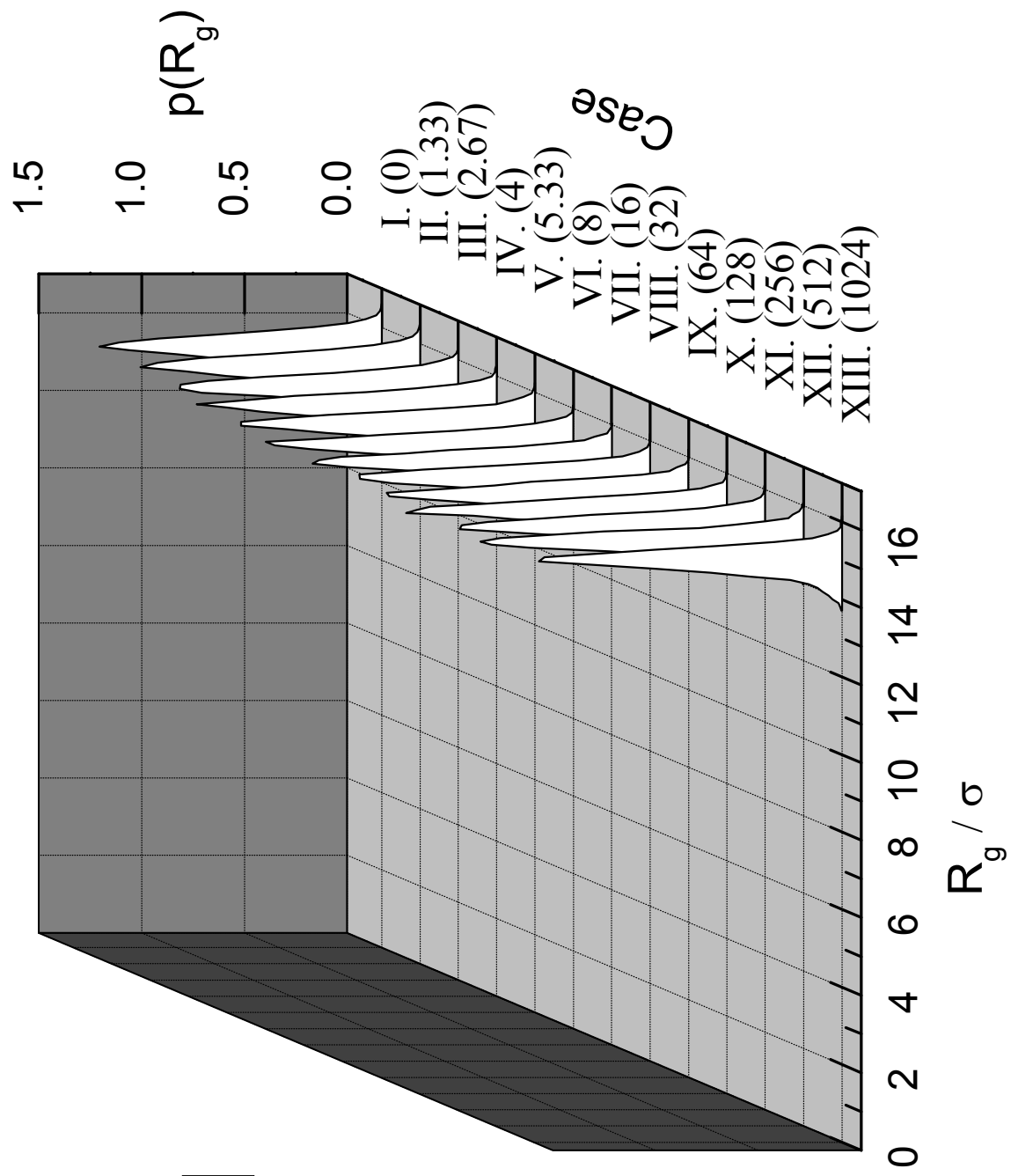


FIG. 10: (b)

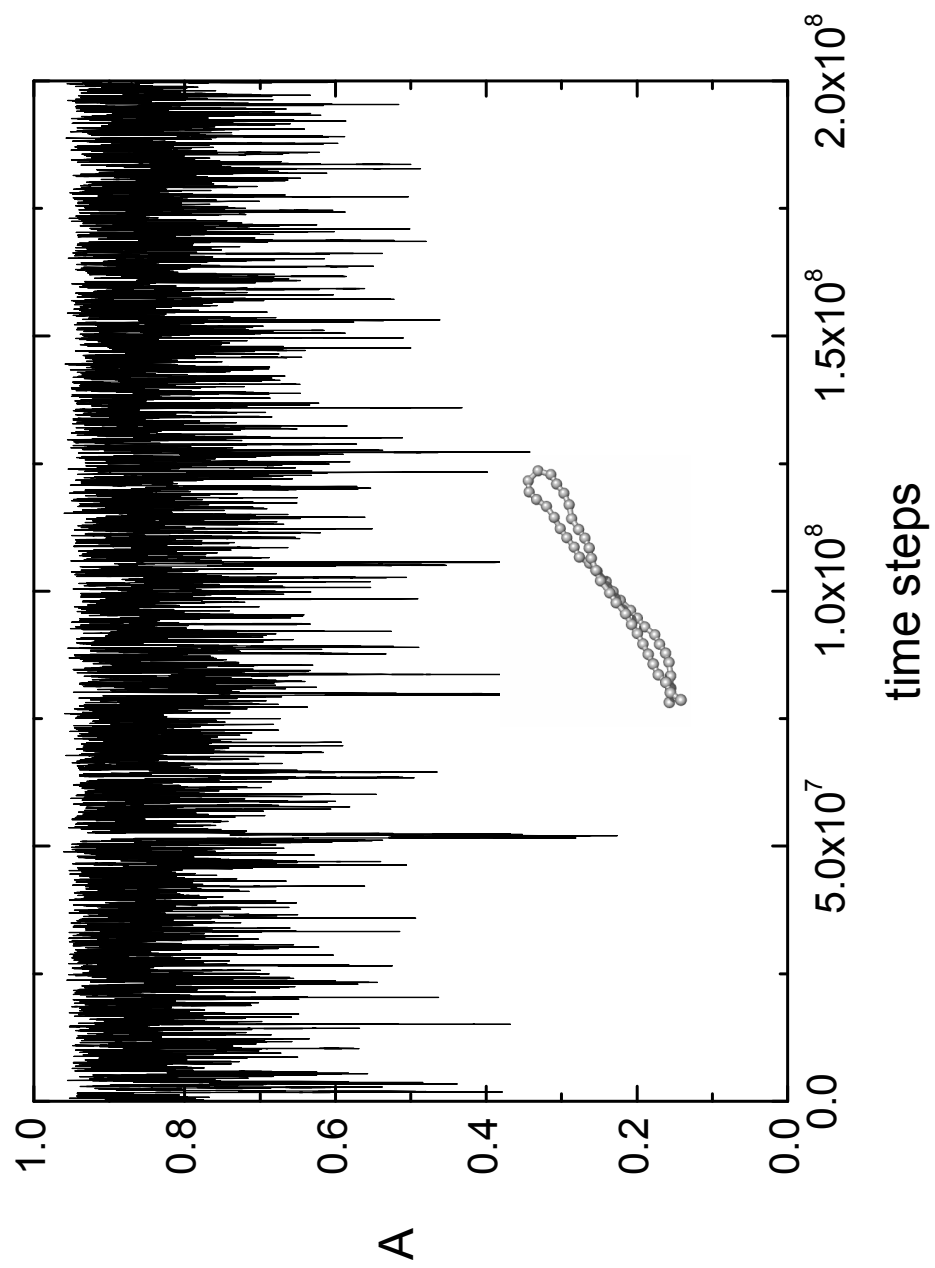


FIG. 11: (a)

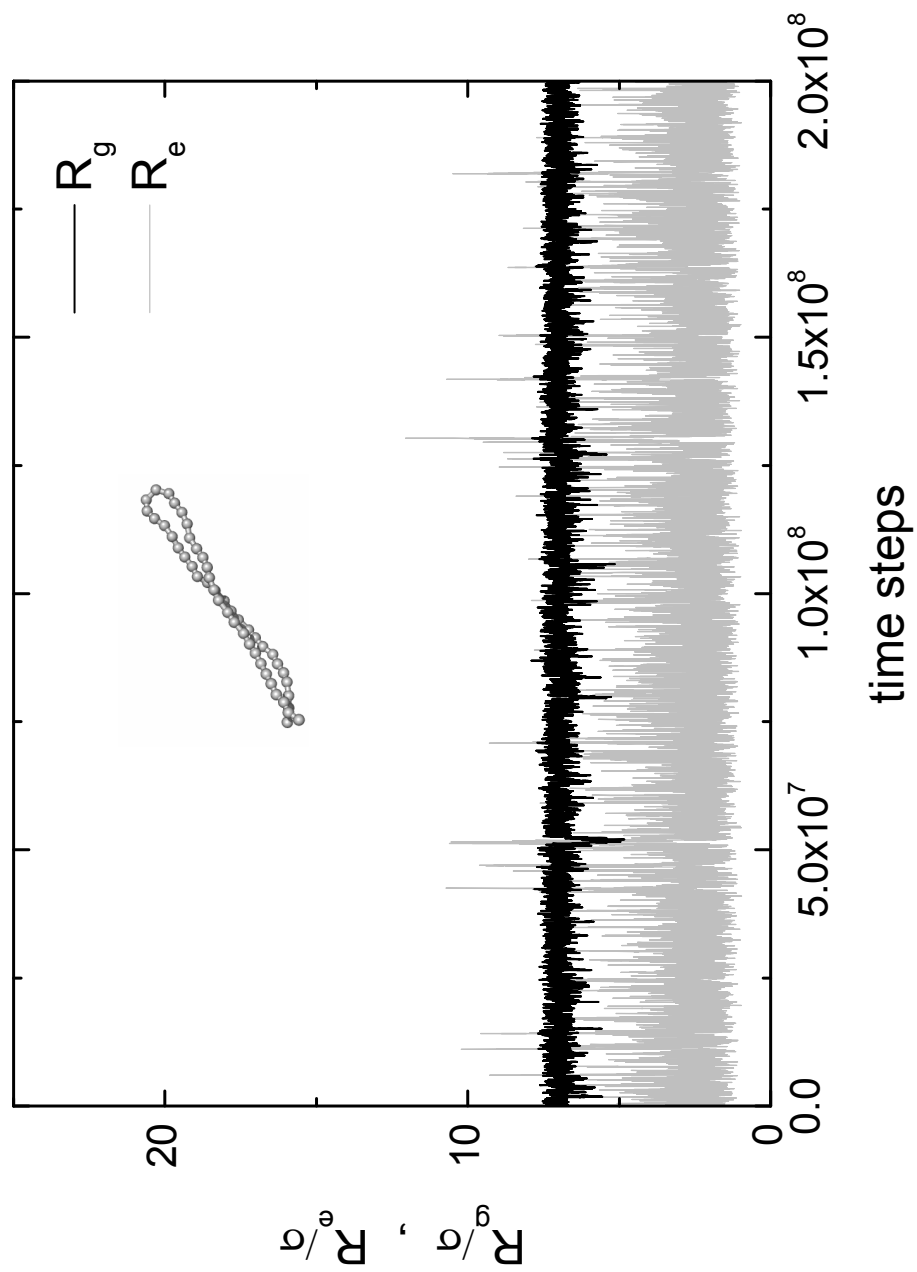


FIG. 11: (b)

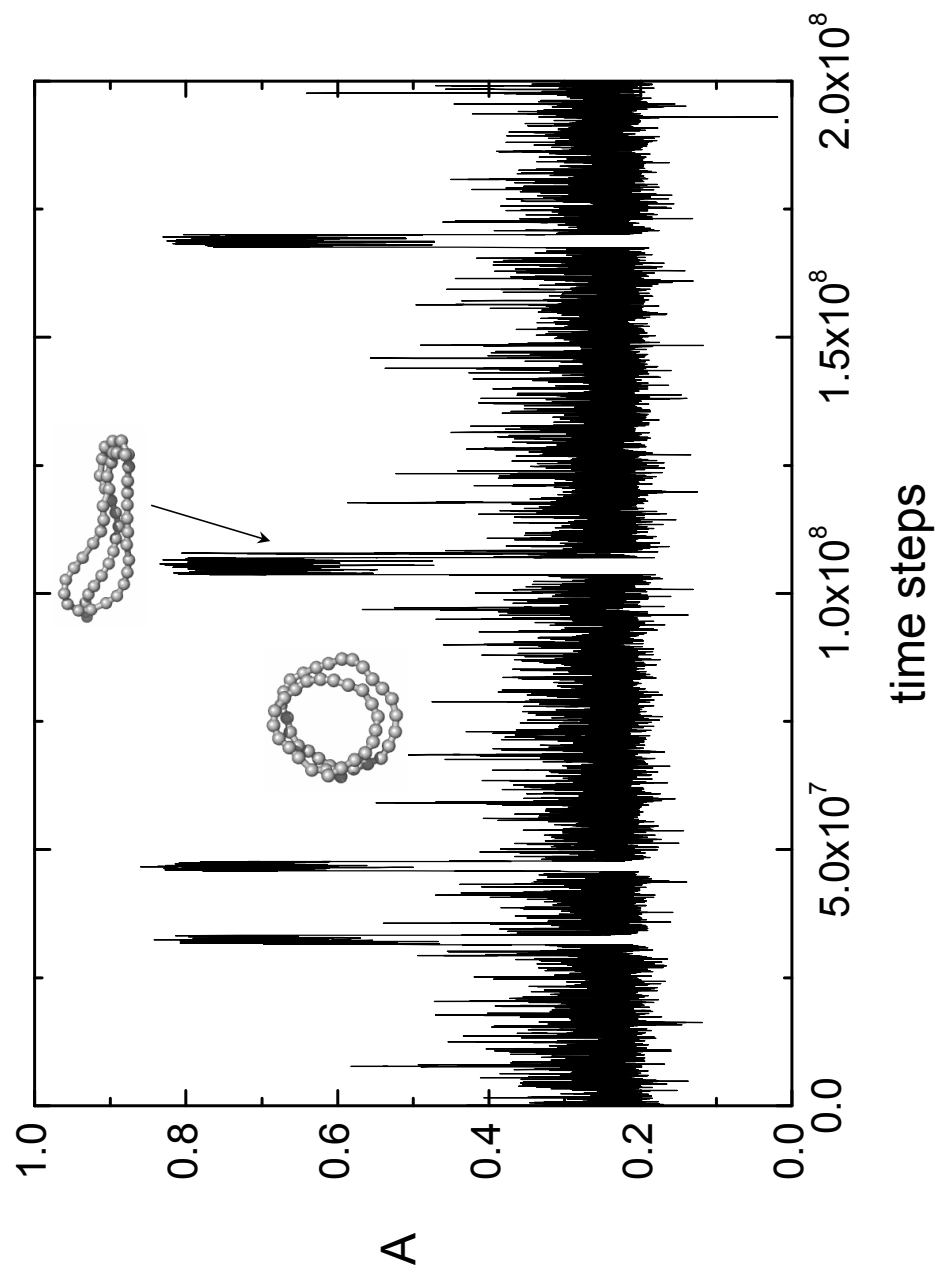


FIG. 12: (a)

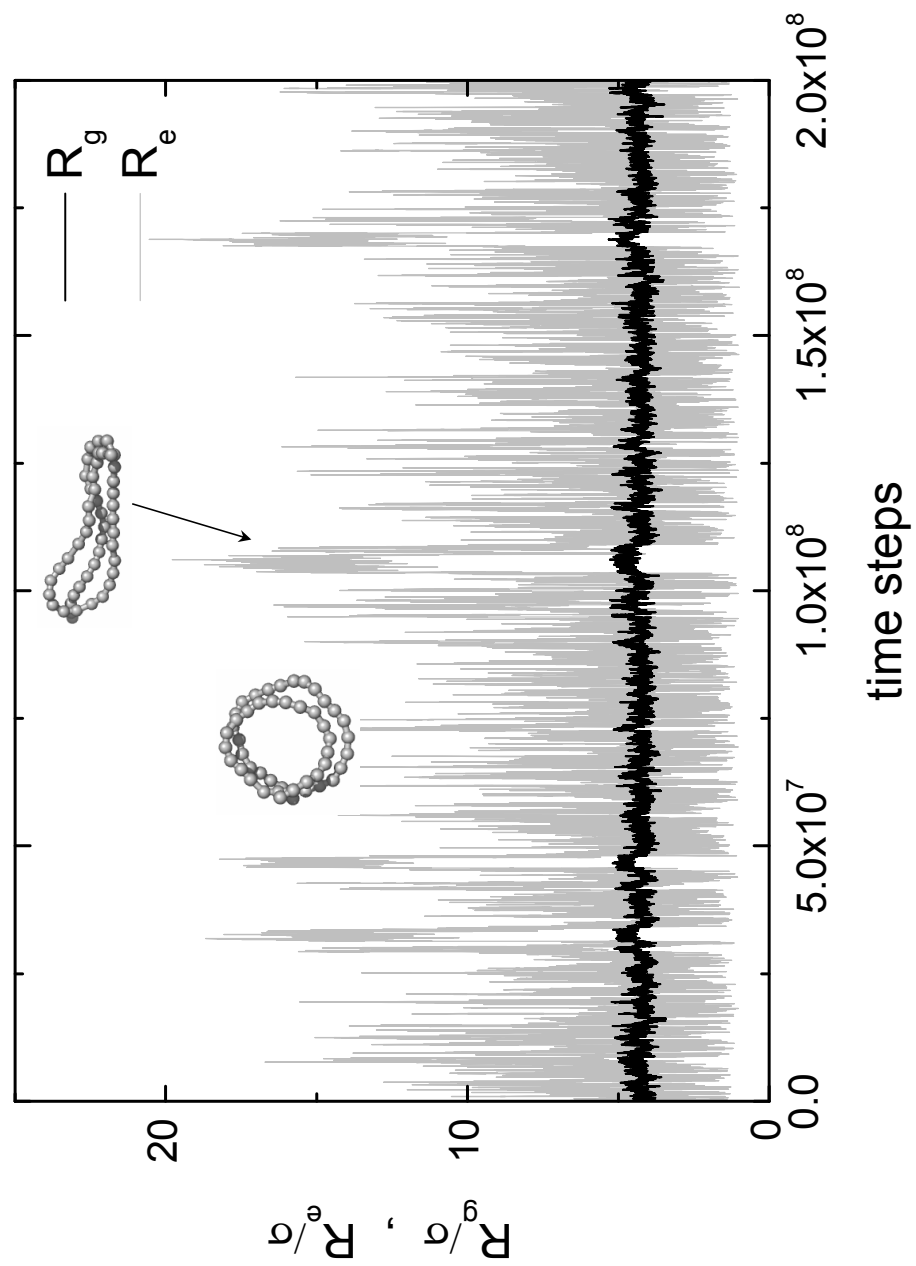


FIG. 12: (b)

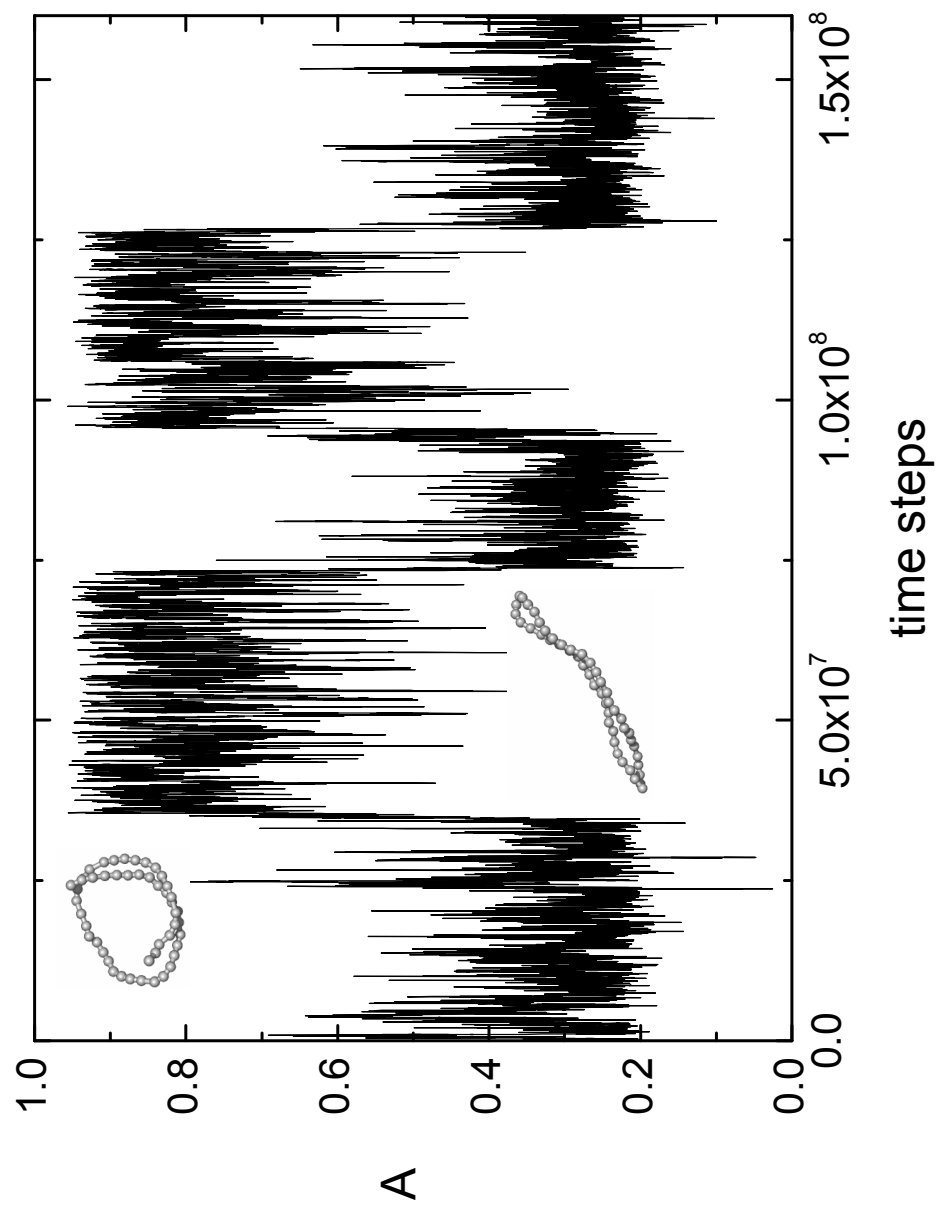


FIG. 13: (a)

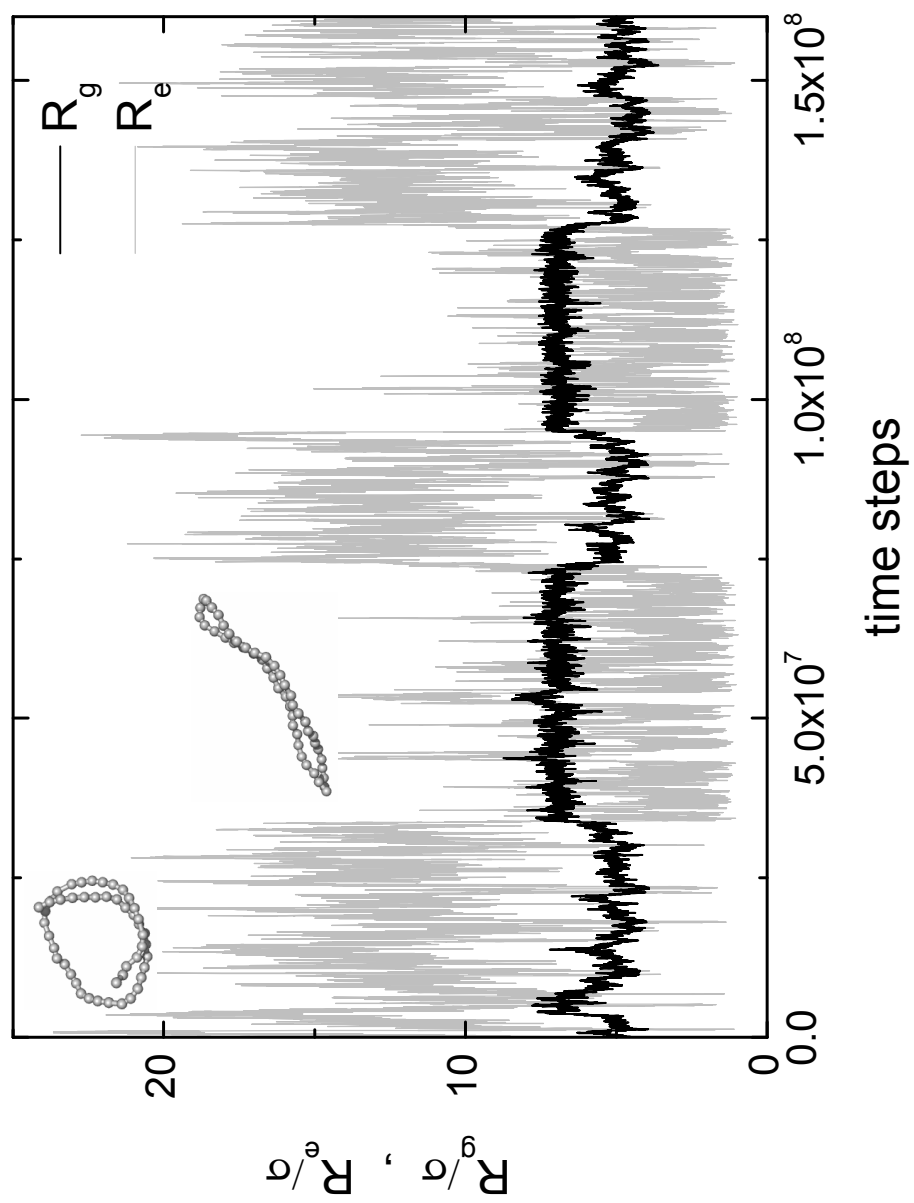


FIG. 13: (b)

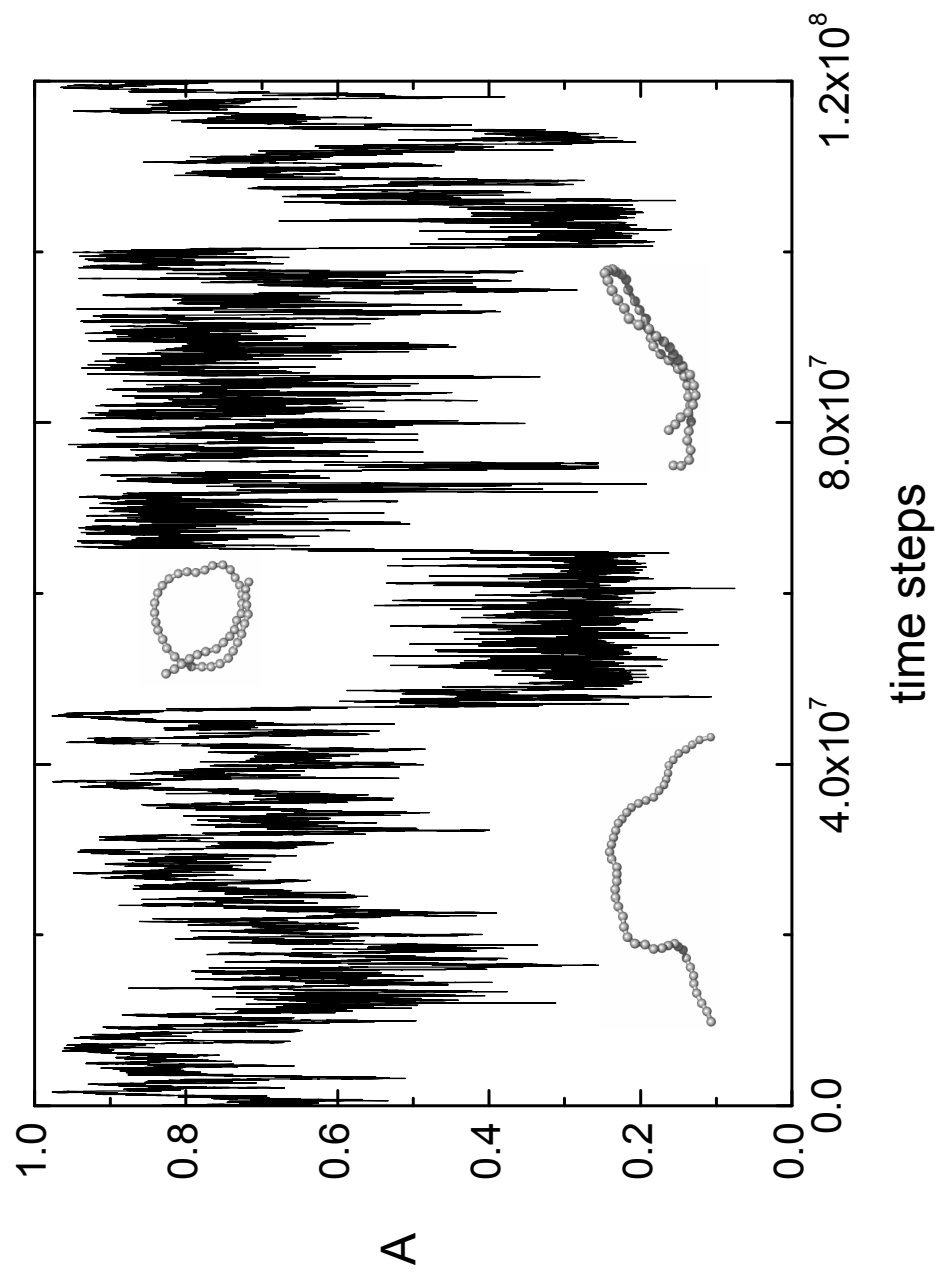


FIG. 14: (a)

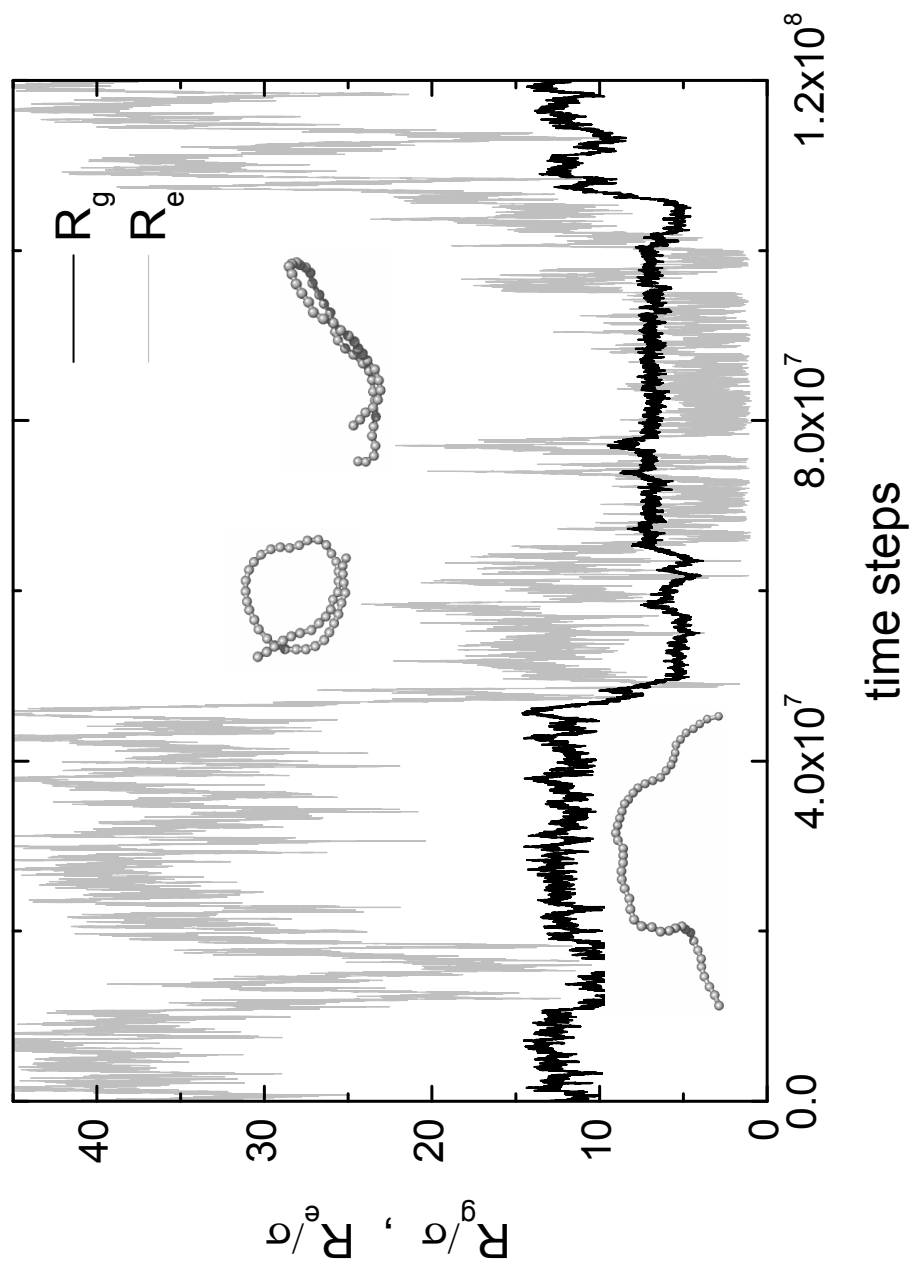


FIG. 14: (b)

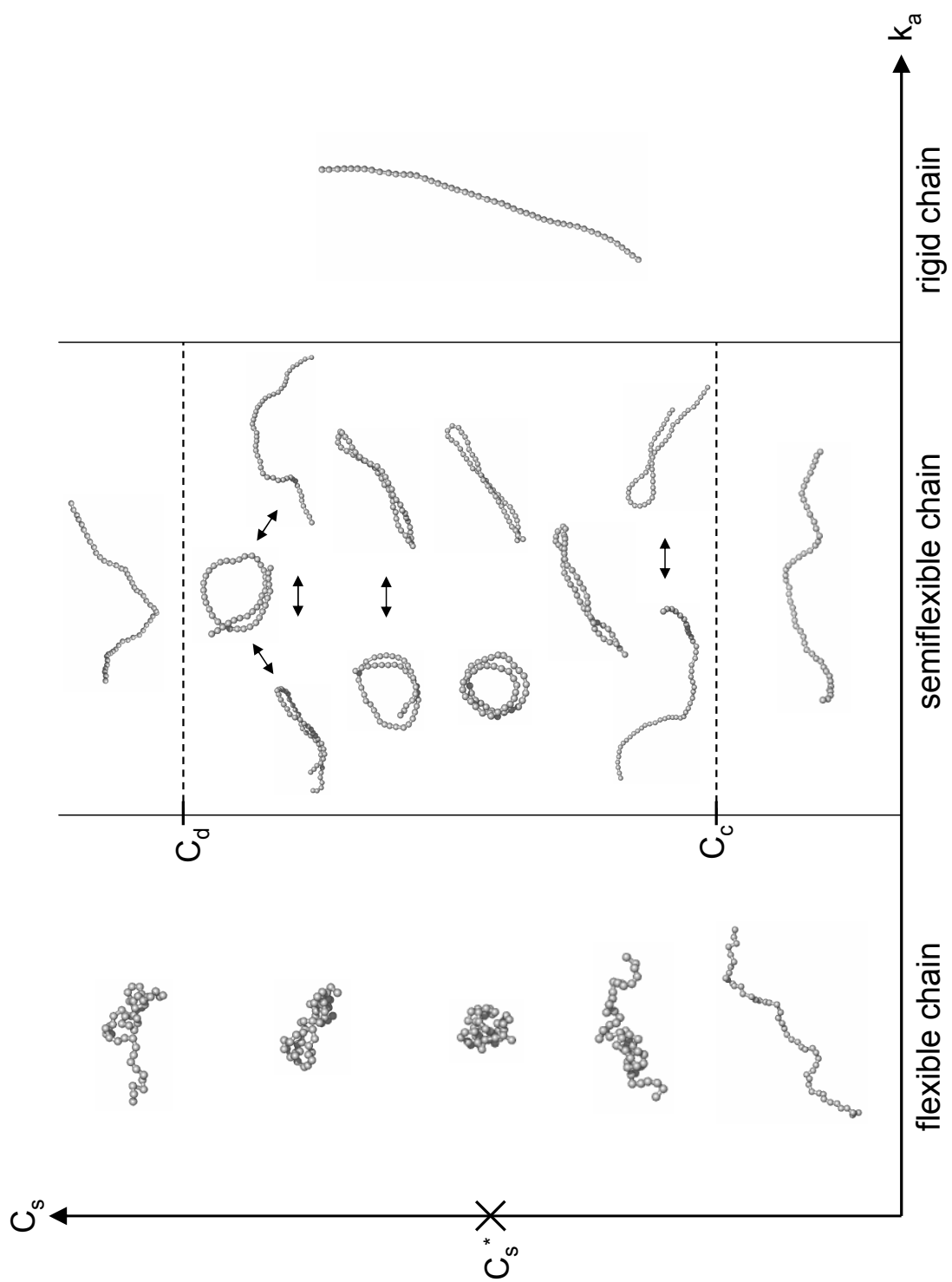


FIG. 15: